A CFD Analysis of Ocean Destratification by Monopile Wind Turbine Foundations:

Comparing Regular and Perforated Designs

R.J. (Robbert) Lip

Technische Universiteit Delft

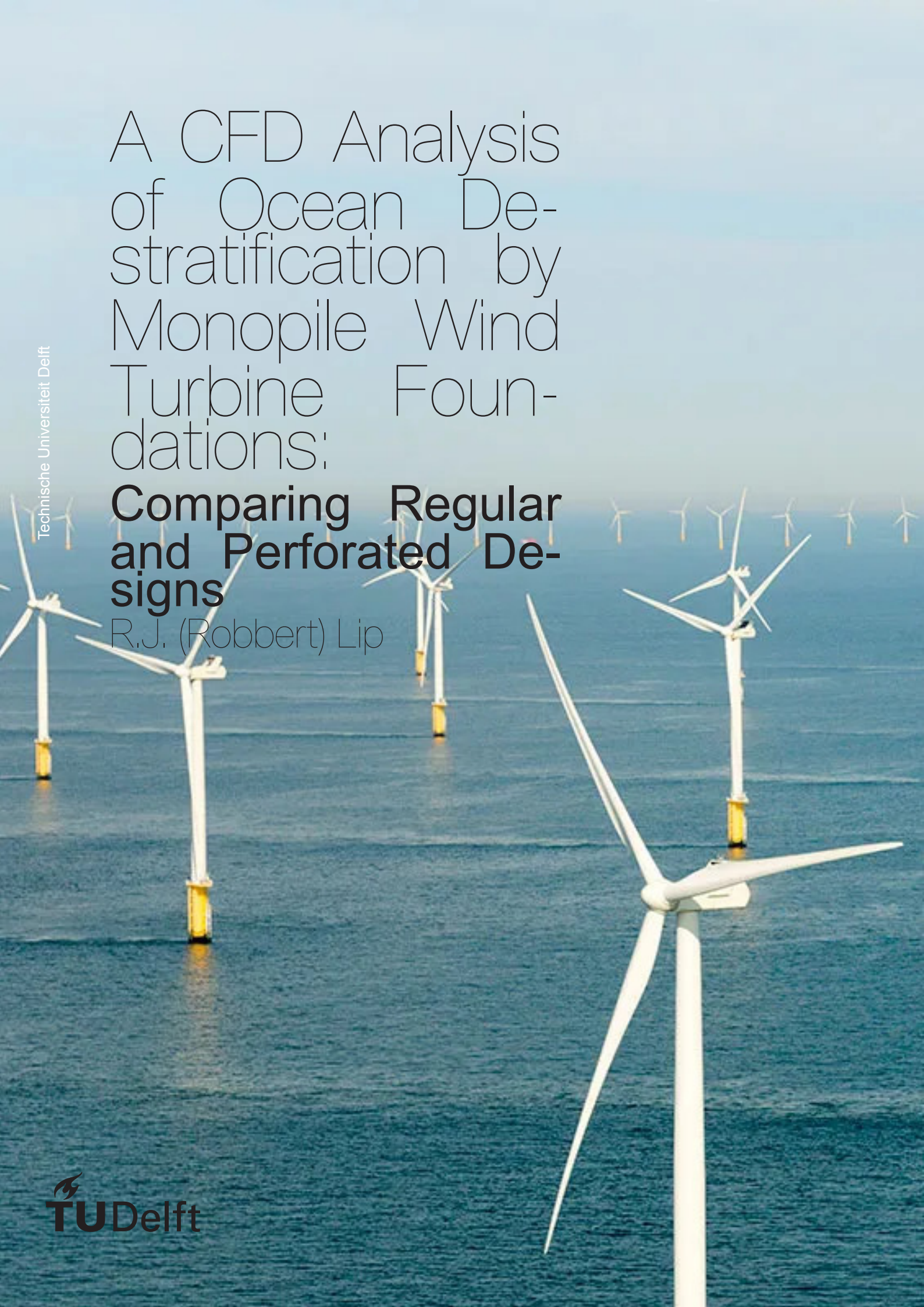

TU Delft

A CFD Analysis of Ocean Destratification by Monopile Wind Turbine Foundations:

Comparing Regular and Perforated Designs

by

R.J. (Robbert) Lip

to obtain the degree of Master of Science,

in the field of Civil Engineering - Hydraulic Engineering,

at the Delft University of Technology,

to be defended publicly on 26-03-2025 at 10:00

Student number:	4906098	
Project duration:	November, 2024 – March 26, 2025	
Thesis committee:	J.O. Colomés Gene,	TU Delft, Chairman Committee
	T.C. Raaijmakers,	TU Delft, Committee Member
	W.S.J Uijttewaal,	TU Delft, Committee Member
	M. Collin,	TotalEnergies, Company Supervisor
	O. Roussel,	TotalEnergies, Company Supervisor

An electronic version of this thesis work is available at: http://repository.tudelft.nl/.

TU Delft

TotalEnergies

Preface

The completion of this thesis marks the end of an enriching academic journey at Delft University of Technology. Throughout this period, I have had the chance to explore the fascinating world of civil engineering, particularly in the fields of hydraulic engineering and offshore wind energy.

The aim of this work was to assess whether a newly designed monopile could help mitigate the destratification of seawater, reducing its potential impact on marine ecosystems. Conducted in collaboration with TotalEnergies R&D Wind in Paris, this research has not only pushed me academically but has also given me a glimpse into the real-world applications of engineering in offshore wind development.

None of this would have been possible without the support and guidance of many people. First, I would like to express my sincere gratitude to my TU Delft supervisors, Oriol Colomés Gene, Tim Raaijmakers, and Wim Uijttewaal for their continuous support, insightful discussions, and valuable feedback. Their expertise and encouragement have been crucial in shaping this research.

I would like to extend my appreciation to my TotalEnergies supervisors, Magali Collin and Olivier Roussel, for their technical guidance, mentorship and for providing industrial insights that enriched my understanding of this research.

Beyond academics, I owe a huge thank you to my friends and family for their endless encouragement, their willingness to listen to me talk about monopiles way too often.

Lastly, I hope that the findings of this research contribute to the ongoing discussions on the environmental impact of offshore wind energy and inspire further studies on sustainable engineering solutions for our oceans.

Robbert Lip
Paris, March 2025

Abstract

As offshore wind energy expands, the environmental impact of monopile foundations on ocean stratification has become a growing concern. Thermal stratification occurs when layers of seawater with different temperatures form due to solar heating, creating a stable density gradient that limits vertical mixing. However, monopile-induced turbulence can disrupt this layering, a process known as destratification, which may have significant ecological consequences.

This study investigates a novel perforated monopile design as a potential solution to mitigate these effects. Using Computational Fluid Dynamics (CFD) simulations in OpenFOAM, the research compares the hydrodynamic behavior of regular and perforated monopiles, focusing on turbulence intensity, wake formation, and destratification rates.

The results indicate that perforated monopiles reduce turbulence intensity and modify wake dynamics compared to regular monopiles, by allowing partial water flow through the structure and reducing recirculation zones. However, their impact on destratification rates remains minor. While perforations alter hydrodynamic behavior, they do not significantly mitigate stratification breakdown.

These findings suggest that while perforated monopiles influence flow dynamics, their effectiveness in reducing destratification is not significant enough to definitely recommend these structural modifications. Future research should explore different perforation patterns and other alternatives develop more sustainable offshore wind turbine foundations.

Contents

Preface iii

Abstract iv

List of Figures viii

List of Tables x

Glossary xi
Symbols . . . xi
Abbreviations . . . xi

1 Introduction 1
1.1 Research Context . . . 1
1.1.1 Offshore Monopile Foundations . . . 1
1.1.2 Monopile Induced Hydraulic Turbulence . . . 1
1.1.3 Ocean water stratification . . . 2
1.1.3.1 Thermocline . . . 3
1.1.4 Ecological Impact of Increased Turbulence . . . 3
1.1.5 Perforated Monopiles . . . 4
1.1.5.1 Advantages of Perforations . . . 5
1.1.5.2 Downsides of Perforations . . . 5
1.2 Literature Review . . . 5
1.2.1 Numerical Modeling of Water Flow Around a Monopile . . . 6
1.2.2 Numerical Modeling of Stratification . . . 6
1.2.3 Monopile Induced Mixing and Destratification . . . 7
1.2.4 Perforated Monopile Designs . . . 7
1.3 Gap in the Literature . . . 7
1.4 Research Problem . . . 7
1.5 Research objective . . . 8
1.6 Research Scope . . . 8
1.7 Research Questions . . . 8
1.7.1 Main research question . . . 8
1.7.2 Supporting research questions . . . 8

2 Theoretical Background 10
2.1 Navier-Stokes Equations . . . 10
2.2 The Boussinesq Approximation . . . 10
2.2.1 The Boundary Layer / Law of the Wall . . . 11
2.3 Numerical Approaches . . . 12
2.3.1 Direct Numerical Simulation . . . 13
2.3.2 Large Eddy Simulation . . . 13
2.3.3 Reynolds-Averaged Navier-Stokes . . . 13
2.4 Closure of RANS Equations . . . 14
2.4.1 The Boussinesq Eddy Viscosity Hypothesis . . . 14
2.4.2 Reynolds Stress Model . . . 15

2.5 Spatial Discretization . . . 15
2.5.1 Finite Volume Method . . . 16
2.6 Residuals . . . 16
2.7 Initial and Boundary Conditions . . . 17
2.7.1 Initial Conditions . . . 17
2.7.2 Boundary Conditions . . . 17
2.8 Solution Algorithms . . . 18
2.9 Steady-State or Transient . . . 18
2.10 Parameter Under-Relaxation . . . 19
2.11 OpenFOAM . . . 19

3 Methodology **20**
3.1 Model Choice . . . 20
3.1.1 OpenFOAM . . . 20
3.1.2 RANS . . . 20
3.1.3 Turbulence Model . . . 20
3.1.4 Wall Models . . . 20
3.2 Computational Domain and Grid . . . 21
3.2.1 Dimensions . . . 21
3.2.2 Initial Conditions . . . 21
3.2.3 Boundary Conditions . . . 22
3.3 Cases & Scenarios . . . 22
3.3.1 Cases . . . 22
3.3.2 Scenarios . . . 24
3.3.3 Refinement Strategies . . . 24
3.4 Analysis Methods . . . 24
3.4.1 Velocity Wake . . . 24
3.4.2 Transverse Flow Profiles . . . 25
3.4.3 Turbulence Parameters . . . 25
3.4.4 Relative Destratification . . . 25
3.5 Validation and Verification . . . 26

4 Results **27**
4.1 Model Validation . . . 27
4.1.1 Validation basis . . . 27
4.1.2 Validation . . . 28
4.2 Velocity Wake . . . 28
4.2.1 Regular Monopile . . . 29
4.2.2 Perforated Monopile . . . 29
4.2.3 Velocity Wake Comparison . . . 30
4.2.4 Wind Farm Scale . . . 32
4.3 Transverse Flow Profiles . . . 33
4.3.1 Downflow . . . 33
4.3.2 Downstream transverse profiles . . . 35
4.4 Turbulence Parameters . . . 36
4.4.1 Turbulence Kinetic Energy (TKE) . . . 36
4.4.2 Specific Dissipation Rate . . . 37
4.4.3 Turbulent Eddy Viscosity . . . 38
4.4.4 Combined . . . 38
4.5 Thermal Stratification . . . 39
4.5.1 Regular monopile . . . 39
4.5.2 Perforated Monopile . . . 40
4.5.3 Comparison . . . 40

5 Discussion **42**
5.1 Interpretation of Key Findings . . . 42
5.1.1 Wake and Flow Recovery . . . 42

5.1.2 Transverse Flow Profiles . . . 42
5.1.3 Effect of Initial Stratification . . . 42
5.1.4 Effect of Monopile Design on Destratification . . . 43
5.2 Ecological Implications . . . 43
5.3 Engineering Implications . . . 44
5.4 Assumptions and Limitations . . . 44

6 Conclusion **46**
6.1 Conclusion . . . 46
6.2 Broader Context and Impact . . . 46
6.3 Recommendations for Future Research . . . 47

List of Figures

1.1 Different types of foundations: (a) suction caisson, (b) gravity-based, (c) monopile, (d) jacket on suction caissons, (e) jacket on slender piles, (f) semi-sub, (g) SPAR, (h) barge, (i) TLP, [26] . . . 1
1.2 Sketch of turbulent mechanisms around a vertical pile, [31] . . . 2
1.3 Process of flow separation around a cylinder, figure by [1] . . . 2
1.4 Evolution of the monthly mean potential energy anomaly ϕ, which is a measure for the stratification strength, [12] . . . 3
1.5 Generalized ocean water pycnocline . . . 3
1.6 Perforated monopile design, HWL = High Water Level, MWL = Mean Water Level, LWL = Low Water Level, [4] . . . 4

2.1 Different layers within the boundary layer, divided by green vertical lines, [21] . . . 12
2.2 Different CFD models approaches and their resolving scale . . . 12
2.3 Reynolds averaging, illustrating the fluctuating part of the turbulence u' and the mean $\overline{u}$, [10] . . . 13
2.4 k-omega SST models, a combination between the turbulence models k-epsilon and k-omega, [22] . . . 15
2.5 One grid cell, showing the cell-center and the different faces [19] . . . 16
2.6 Residuals from an OpenFOAM simulation, excluding pressure residuals, plot created using gnuplot . . . 17
2.7 Boundary conditions on a rectangular computational domain, with a monopile cylinder inside . . . 18
2.8 Parameter under relaxation, [20] . . . 19

3.1 Top view of the computational domain, with the white hole representing the monopile . . . 21
3.2 Side view of the domain with the initialized temperature . . . 22
3.3 Boundaries of the computational domain . . . 22
3.4 Regular monopile used in this research, including dimensions . . . 23
3.5 Perforated monopile used in this research, including dimensions . . . 23
3.6 Computational grid for the perforated monopile, showing the refinement around the monopile 24
3.7 Vertical temperature profile at three locations, x = -50 m (red), x = 100 m (green) and x = 500 m (blue). T(-50, 0, 32) - T(500, 0, 32) and ΔT are visualized . . . 26

4.1 Turbulence Kinetic Energy over downstream direction until 3000 m downstream . . . 28
4.2 Top view of the velocity wake for the Regular monopile, flow direction is rightward, up to 1000 m downstream, values in [m/s] . . . 29
4.3 Side view of the velocity wake for the Regular monopile through the center of the monopile, flow direction is rightward, slice up to 300 m downstream, values in [m/s] . . . 29
4.4 Top view of the velocity wake for the Perforated monopile, flow direction is rightward, up to 1000 m downstream, values in [m/s] . . . 29
4.5 Side view of the velocity wake for the Regular monopile, flow direction is rightward, slice up to 300 m downstream, values in [m/s] . . . 30
4.6 Process of flow separation around a cylinder, with the purple arrow (not on scale) depicting the flow through the perforations, figure by [1], edited by author . . . 30

4.7 Velocity magnitude of the Perforated and Regular monopile of the downstream (x) direction, 0.5 m under the waterline and through the center of the monopile. The black line demonstrates the point where 90% of the free stream velocity is recovered, which is at 660 m downstream for the regular monopile and 210 m downstream for the perforated design . . . 31
4.8 Close up wake of the regular and perforated monopiles, values in [m/s] . . . 31
4.9 Front view of the velocity for both monopiles, flow direction into the paper, values in [m/s] 32
4.10 Vector field of the velocity, x-component is divided by 15 to be able to visualize the y- and z-components of the velocity, the figure does not show a scale as this has no meaning because of the recalculation of the velocity field. Red indicated high and blue indicates low yz-directed velocities . . . 32
4.11 Wakes of 1000 m of the regular monopile design in the Borselle III wind farm, with monopiles diameters or around 7 to 8 m. Figure from [51], adapted by author. . . . 33
4.12 Vector visualization of the downflow in front of the monopiles. The horizontal component of the velocity is divided by 1200 to visualize the vertical components, the scale shows the z-directed velocity magnitude . . . 33
4.13 Upward directed flow velocity (downward is negative) over depth for the regular and perforated designs, 5 m in front of the monopile vertical centerline, meaning 1.5 m in front of the monopile (D = 7 m) . . . 34
4.14 Streamlines of the flow upstream of one of the holes. Longer arrows mean higher velocities. This is not on scale. u_∞ = free-stream velocity. . . . 35
4.15 Vector visualization of y- and z-components of the flow, 100 m downstream of the monopiles, scales show the yz-directed velocity magnitude . . . 36
4.16 Turbulence Kinetic Energy of the Perforated and Regular monopile of the downstream (x) direction through the center of the monopile. . . . 36
4.17 Turbulence Kinetic Energy in the wake of the Regular monopile (top) and the perforated monopil3 (bottom), z-slice (top view) . . . 37
4.18 Close-up Turbulence Kinetic Energy wake of the regular and perforated monopiles, z-slice at a water depth of 2 m . . . 37
4.19 Side views (y-slices) of the Turbulence Kinetic Energy Wake of the regular and perforated monopiles . . . 37
4.20 Specific Dissipation Rate ω of the Perforated and Regular monopile of the downstream (x) direction through the center of the monopile at an elevation of z = 25 m. The peak of $\omega_{perforated}$ extends until 0.9 [1/s] . . . 38
4.21 Turbulent Eddy Viscosity ν_t of the Perforated and Regular monopile of the downstream (x) direction through the center of the monopile . . . 38
4.22 ν_t, TKE and ω for the regular monopile combined in one figure, until 3000 m downstream 39
4.23 Top view and side view of the temperature in the computational domain for the regular monopile . . . 39
4.24 Top view and side view of the temperature in the computational domain for the perforated monopile . . . 40
4.25 Absolute destratification for the regular and perforated designs for different stratification strengths . . . 41
4.26 Relative Destratification for the regular and perforated designs for different stratification strengths . . . 41

List of Tables

3.1 Wall models used in this research 21
3.2 Dimensions of the Computational Domain 21
3.3 Initial conditions 21
3.4 Boundary Conditions for T, U and pressure. Excluding k, omega, alphat and nut 22

4.1 RET and TRL for D = 7 m 28
4.2 RET comparison between [39] and the numerical model in this research 28
4.3 Simulation results of the regular monopile, showing the Relative Destratification, see subsection 3.4.4. The values are in Kelvin, except when stated differently 40
4.4 Simulation results of the perforated monopile, showing the Relative Destratification, see subsection 3.4.4. The values are in Kelvin, except when stated differently 40

Glossary

Variables and symbols

ρ	Material density	$[kg/m^3]$
∇	Nabla operator or Divergence	[-]
ρ_w	Water density	$[kg/m^3]$
u	Velocity component	$[m/s]$
p	Pressure	$[kg/ms^2 = Pa]$
E	Energy	$[m^2/s^2]$
τ	viscous stress tensor	$[kg/ms^2]$
k	Thermal conductivity	$[W/mK]$
T	Temperature	$[K]$
Re	Reynolds number	[-]
δ_{ij}	Kronecker delta	[-]
μ	Dynamic viscosity	$[kg/ms = Ns/m^2]$
ν	Kinematic viscosity	$[m^2/s]$
u_∞	Free-stream velocity	$[m/s]$

Abbreviations

CFD	Computational Fluid Dynamics
SST	Shear Stress Transport
TKE	Turbulence Kinetic Energy
TKE_0	Background Turbulence Kinetic Energy
RTA	Relative Temperature Anomaly
RD	Relative Destratification
EDS	Empty Domain Destratification
RET	Relative Excess Turbulence
TRL	Turbulence Recovery Length Scale

1 Introduction

1.1. Research Context

The offshore wind industry is growing rapidly due to the rising demand in renewable energy sources. According to [23], the global offshore wind energy capacity is expected to reach 330 gigawatts (GW) by 2030 and 1 terawatt (TW) by 2050. Offshore wind farms, particularly those using monopile foundations, have become a common sight in shallow sea areas. 80.5% of all offshore turbine installations in 2020 consist of monopile foundations [52]. During summer months, certain areas develop a strong thermal stratification. [32] Tidal motion interacting with the foundations create a hydraulic wake which could alter this vertical thermal stratification profile, potentially having negative effects on marine life.

1.1.1. Offshore Monopile Foundations

Offshore monopile foundations, for which Figure 1.1 (c) is an example, are a common structural solution for supporting wind turbines in shallow to intermediate water depths. These cylindrical steel structures are driven into the seabed to provide stability against environmental loads, such as wind, waves, and currents.

Design and Installation

Monopiles can be either uniformly cylindrical or tapered. The wall thickness varies between 40 mm and 120 mm and is dependent on load requirements, usually with thicker profiles near the bottom and slimmer parts near the top. The diameter of the substructure usually range between 5 m and 10 m. Larger substructures are used for supporting turbines with capacities exceeding 10 MW.

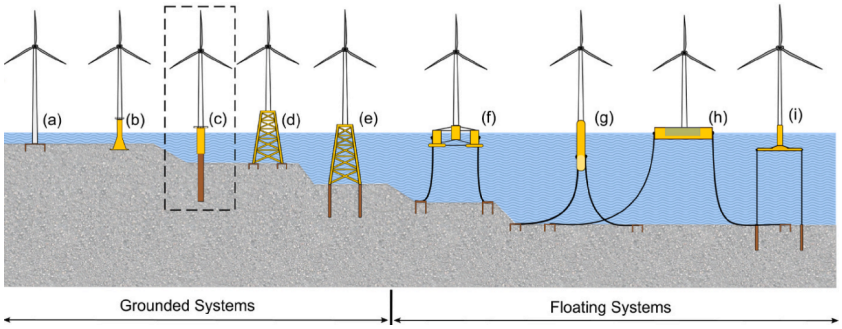

Figure 1.1: Different types of foundations: (a) suction caisson, (b) gravity-based, (c) monopile, (d) jacket on suction caissons, (e) jacket on slender piles, (f) semi-sub, (g) SPAR, (h) barge, (i) TLP, [26]

Usually, monopiles are driven 20 m to 40 m into the seabed. In softer soils, they might have to be driven deeper into the bed. Monopile substructures are feasible in water depths up to 50 meters. For medium water depth (50-80 m) a jacket substructure suits better. Going even deeper, floating wind is a more competitive. [33]

1.1.2. Monopile Induced Hydraulic Turbulence

Flow around a vertical pile is a complex, three-dimensional process, which can be observed from Figure 1.2. When water flows toward a vertical pile, it encounters an obstruction, reducing flow velocity

to zero at the upstream face of the pile. This creates a high-pressure zone on the pile's upstream side, generating a pressure gradient that opposes the flow direction. In the far field, the flow is assumed to follow a logarithmic vertical profile, with both velocity and pressure on the pile face decreasing from the surface down to the bed. This induces a downflow. This causes the bed boundary layers to separate, leading to horseshoe vortices. These horseshoe vortices create a high bed shear stress, leading to localized sediment removal, or scour, near the base of the pile. Along the pile, the flow will separate and create lee-wake vortices [31].

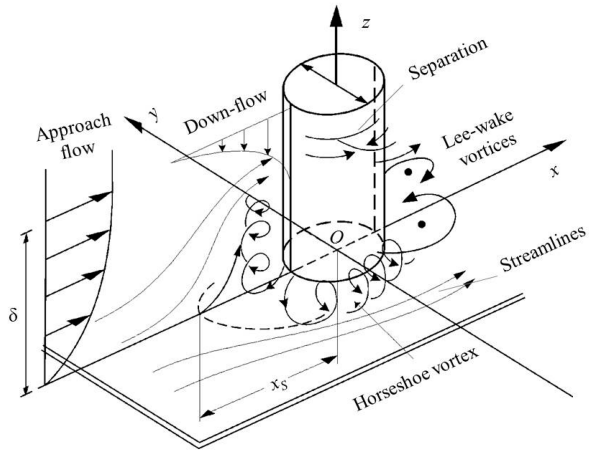

Figure 1.2: Sketch of turbulent mechanisms around a vertical pile, [31]

The process of flow separation is shown in a top view in Figure 1.3. The water in the boundary layer moves slower compared to the water further away from the cylinder. This causes flow to recirculate and eventually separate.

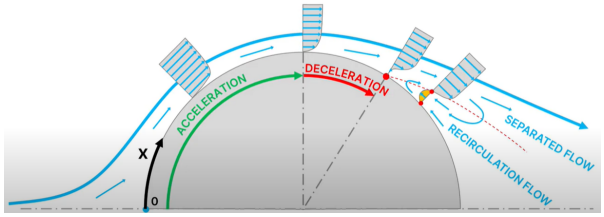

Figure 1.3: Process of flow separation around a cylinder, figure by [1]

Monopile-induced turbulence significantly enhances sediment suspension in the surrounding water column, creating visible sediment plumes downstream.

Suspended sediment
Monopile-induced turbulence enhances sediment suspension in the water column, leading to visible sediment plumes downstream. As water flows around a monopile, vortices such as horseshoe vortices near the seabed and wake vortices downstream increase bed shear stress. This elevated stress mobilizes sediment particles from the seabed, which are then transported and dispersed by turbulent mixing and ambient currents. Fine sediments, in particular, remain suspended for extended periods, forming plumes that extend far downstream [47].

1.1.3. Ocean water stratification

Thermal ocean stratification is the layering of ocean water into horizontal sections based on density differences. This layering tends to remain stable because warmer, less dense water stays on top of the cooler, more dense water [30]. The development of thermal stratification in the North Sea is primarily driven by solar radiation competing with mixing from tidal currents, surface wind stress [42]. Convection, so warmer water rising and cooler water sinking, strengthens stratification. Stratification is present in all

bodies of water, where it acts as an obstruction to mixing of water, which affects the exchange of heat, carbon, oxygen and nutrients. Figure 1.4 presents the variation of the thermal stratification strength in the North Sea over a year in 2018, indicating that during the summer months the stratification is strongest.

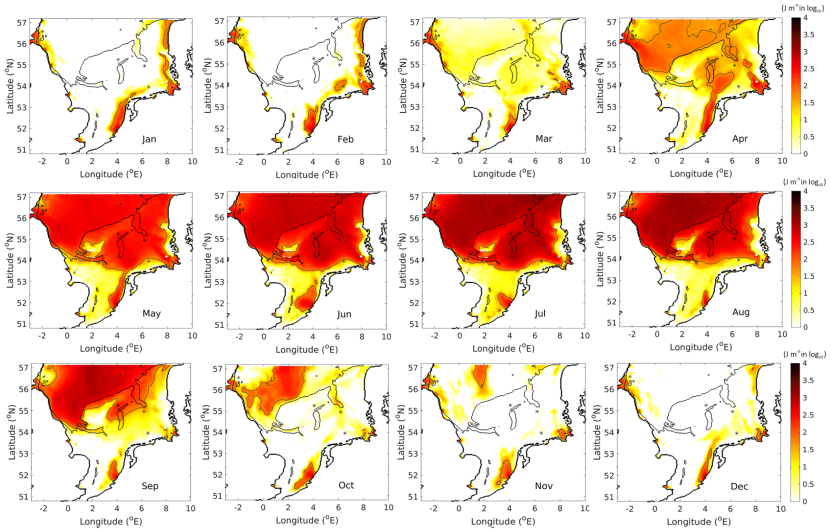

Figure 1.4: Evolution of the monthly mean potential energy anomaly ϕ, which is a measure for the stratification strength, [12]

1.1.3.1 Thermocline

Figure 1.5 shows a clear pycnocline, meaning the layer with the strongest density gradient $\frac{\partial \rho}{\partial z}$ over the depth. For a constant salinity this corresponds to a thermocline. The thermocline commonly coincides with the pycnocline [17]. The mixed layer above the thermocline is the epilimnion and the deep layer below the thermocline is the hypolimnion. The epilimnion is characterized as relatively homogeneous, containing most oxygen and being nutrient-rich.

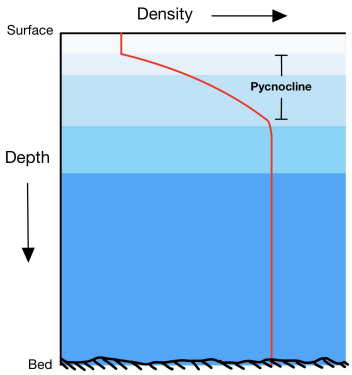

Figure 1.5: Generalized ocean water pycnocline

1.1.4. Ecological Impact of Increased Turbulence

Phytoplankton growth

Temperate or oceanic climates are found in both hemispheres, typically between latitudes 40°and 55°, with prominent examples in Northwest Europe, Northwest North America, Tasmania, and New Zealand [46]. Phytoplankton growth in temperate seas is often closely linked to the development of water column stability during spring, which creates a well-lit surface layer that supports rapid spring blooms [45]. This increased production can be an important source of food for a big portion of the pelagic and benthic food chains [48]. Pelagic species being species swimming and floating in the water column and

benthic species being organisms living in and on the bottom [50].

Several sources state that increased mixing only has negative effects as it increases the suspended sediment content in the water column, resulting in less light intrusion. Furthermore, as it could disrupt the water column stability, it could take phytoplankton out of the well-lit photic zone. Other sources state that increased mixing could lead to nutrient enrichment, as the vertical mixing supplies the phytoplankton with enough nutrients like nitrates, phosphates and silicates. Other researchers have stated that, for depths applicable to monopile substructures, the entire water column is well-lit, so stratification has positive effect. [28]

Cold underlayer
On the U.S. East Coast, there is a strong seasonal stratification. The strong thermocline overlies cold (usually < 10°C) water above the bottom. This cold layer is home to boreal fauna that extend farther south than expected if only considering the latitude. Many clam, scallop and fish species benefit from this ”cold pool,” according to [32].

Summary
Potential negative effects of increased mixing:

- Increased suspended sediment leading to less light intrusion
- Increased mixing could take phytoplankton out of the photic zone
- Increased mixing could destroy the cold underlayer, which is home to many species

Potential positive effects of increased mixing:

- Increased mixing could lead to increased nutrient supply
- Increased mixing could increase oxygen levels in the lower part of the water column

1.1.5. Perforated Monopiles

Perforated monopiles are a novel adaptation of traditional monopile foundations used in offshore wind turbine installation. The perforated designs are currently under investigation and are not deployed yet. These monopiles incorporate strategically placed perforations, in the splash zone between the high-water line (HWL) and low-water line (LWL), as shown in Figure 1.6. This section will go into advantages and downsides of perforations in monopiles.

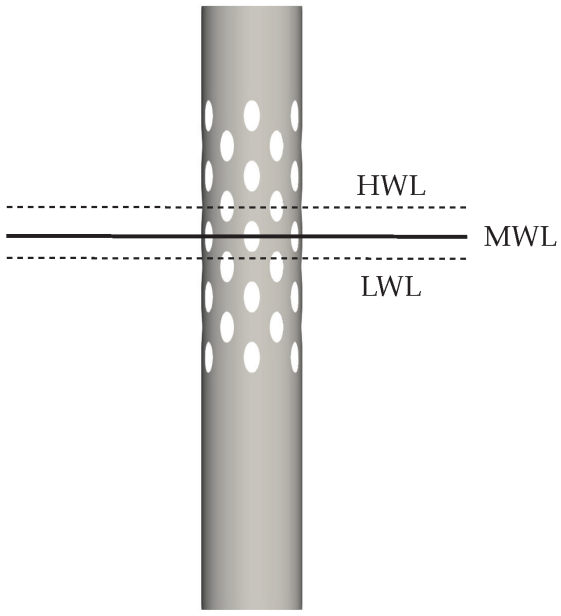

Figure 1.6: Perforated monopile design, HWL = High Water Level, MWL = Mean Water Level, LWL = Low Water Level, [4]

1.1.5.1 Advantages of Perforations

Load Mitigation

Perforations in monopiles can significantly reduce hydrodynamic loads by altering the way water interacts with the structure. By allowing water to flow through the monopile instead of forcing it to entirely divert around the structure, perforations decrease the drag and inertia forces that waves and currents exert on the monopile. This design innovation could enhance structural efficiency and reduce fatigue damage over the operational lifetime of offshore wind turbines. [4]

Marine Life

Perforations in monopiles create sheltered environments that serve as artificial reefs. These structures could attract and support a variety of marine organisms. [37] The circulation of water also prevents the formation of stagnant zones, which could otherwise discourage marine life colonization. Perforated monopiles increase structural complexity, which is known to promote biodiversity by providing diverse micro-habitats. This complexity mimics natural reef environments, encouraging colonization by species.[35]

Corrosion Control

Perforations in monopiles could also play a crucial role in improving corrosion control. The open design allows for consistent water chemistry between the internal and external environments of the monopile, reducing the risk of differential aeration corrosion, a common issue in sealed monopiles. Furthermore, the free circulation of seawater enhances the effectiveness of cathodic protection systems, such as sacrificial anodes or impressed current systems, ensuring uniform protection across the structure. [37]

1.1.5.2 Downsides of Perforations

Structural

Perforations introduce stress concentrations around the edges of the openings, potentially reducing the structural integrity of the monopile. This weakening can lead to increased susceptibility to fatigue and crack propagation, especially under cyclic loading from waves and currents. It can also lead to a reduction in overall load-bearing capacity, requiring careful design to ensure the monopile remains structurally robust. [38]

Installation

Perforations can complicate the installation process, particularly during pile driving. The open structure may increase stresses on the monopile during installation, as the perforations can lead to non-uniform load distribution. This may require adjustments to traditional installation methods, such as using specialized hydraulic hammers or alternative methods like vibro-hammers to mitigate stress concentrations.

Biofouling

The perforations, while beneficial for ecological purposes, can also promote the accumulation of marine organisms (biofouling) on the interior surfaces. This could change the hydrodynamic properties of the monopile over time, potentially increasing drag. It could also lead to maintenance requirements for cleaning and inspecting the internal surfaces.

Higher Manufacturing Complexity

Besides that, perforated cylinder designs require a more advanced manufacturing process, when compared to regular monopiles. They need specialized cutting or shaping methods to create the perforations without destroying material or compromising material properties. Also, they might need additional structural reinforcements to be placed around to perforations.

1.2. Literature Review

The goal of this literature review is to provide a thorough understanding of the current state-of-the-art in the field of offshore wind turbine monopile designs and their impact on sea water stratification. By summarizing the existing research, identifying gaps, and establishing the context for the current study, this review aims to highlight the significance and novelty of the present research. This will set the

stage for a detailed investigation into the effects of regular and perforated monopile designs on sea water stratification, contributing to the development of more environmentally sustainable offshore wind turbine foundations.

1.2.1. Numerical Modeling of Water Flow Around a Monopile

In 2023, a research was done on a nested numerical simulation approach to study the hydrodynamics around monopile foundations of offshore wind farms at Weihai Coastal Water, China. It integrates the large-scale hydrodynamic model TELEMAC with the small-scale OpenFOAM code to capture multi-scale spatial and temporal characteristics of ocean conditions. The model is validated with field measurements and used to analyze the effects of wind speed, direction, and tidal flow on hydrodynamics around the monopile. Key findings include the significant impact of monopile structures on local flow fields and the importance of considering these effects in design and operation to ensure safety and efficiency. [56]

The 2022 paper investigates the three-dimensional (3D) flow around a monopile with scour protection under steady current conditions using a hydrodynamic model based on Volume-averaged Reynolds-averaged Navier-Stokes (VARANS) equations with a volume-averaged k-ω turbulence closure. Implemented in OpenFOAM, the model is validated against experimental data and analytical expressions. The study evaluates flow behaviors inside and outside the scour protection, using a parabolic transition near the interface for accuracy. Results show the model's effectiveness in predicting flow features, highlighting the significant impact of scour protection on local hydrodynamics. [55]

A paper by Jiang from 2023 compares Reynolds-Averaged Navier-Stokes (RANS) and Unsteady Reynolds-Averaged Navier-Stokes (URANS) turbulence models for simulating flow past a circular cylinder using OpenFOAM. The study evaluates the performance of these models in capturing steady and unsteady flow features. Simulations are conducted using the PISO, SIMPLE, and PIMPLE algorithms. Results show that the PISO algorithm effectively simulates unsteady flow at Reynolds numbers 100 and 3900 in 2D, while PIMPLE performs well for unsteady flow at Reynolds numbers 100 and 3.5e5 in 3D. The SIMPLE algorithm, however, is less suitable for steady flow at these Reynolds numbers. The study highlights the strengths and limitations of each model, with comprehensive analyses of force coefficients. [25]

The 2024 paper titled "3D Numerical Modeling of Wave–Monopile–Seabed Interaction in the Presence of a Scour Hole" investigates the impact of scour holes on seabed stability around monopile foundations. Using a 3D numerical model within the OpenFOAM framework, the study analyzes 3D flow velocities, dynamic wave loads, pore pressures, soil effective stresses, and wave forces around a monopile with a scoured profile. Key findings include

1. Reduced pore pressure within the scoured seabed compared to a flat seabed.
2. More uniform distribution of liquefaction depth around the monopile when considering the scour hole effect.
3. The effect of scour holes intensifies with higher saturation degrees and shows a pattern of increase followed by a decrease with increasing permeability.

This research provides valuable insights for coastal engineers concerned with wave-induced seabed instability around monopile foundations. [44]

1.2.2. Numerical Modeling of Stratification

A paper from 2008 by Xu et. al investigates the variations in current circulation, salt intrusion, and vertical stratification in the Pamlico River Estuary (PRE) under different river flow and wind conditions using a three-dimensional numerical model. The model was calibrated and verified with data from 2001 and 2003, and eight sensitivity tests were conducted. Results indicate that salinity intrudes further upstream under low flow, downriver wind, and remote-wind-caused water level set-up conditions. Salinity stratification varies across different estuary portions, being enhanced by higher river discharge, downriver wind, and water level set-up. Freshwater discharge and wind are the primary factors controlling the estuary's dynamics, with weak vertical diffusion potentially explaining the bottom hypoxia observed during summer. [54]

A paper by Balas from 2001 presents a three-dimensional baroclinic numerical model for simulating coastal water processes. The model integrates hydrodynamic, transport, and turbulence components using a combination of finite difference and finite element methods. It employs second-order accurate Crank-Nicholson schemes and the $k - \epsilon$ turbulence model to handle vertical eddy viscosities, while horizontal viscosities are treated with the Smagorinsky subgrid model. Application to Turkey's Göksu Lagoon, a shallow, stratified coastal lagoon, demonstrated realistic simulations of salinity, temperature, and velocity profiles over 91 days. The model captured wind-driven stratification and mixing effects, with salinity prediction errors around 1 ppt. It highlights the model's capability in predicting flow patterns and vertical mixing under various environmental forces. [9]

To accurately model the effects of stratification, it is necessary to accurately represent the temperature induced temperature gradient to obtain a stable solution. This requires a high resolution, especially vertically and mainly in the vertical direction.

1.2.3. Monopile Induced Mixing and Destratification

The study released by Austin et. al examines the impact of offshore wind turbine monopile wakes on seabed stress and water column mixing. Data were collected 40 meters downstream of a monopile in the Rhyl Flats Offshore Wind Farm using high-frequency acoustic Doppler current profiler (ADCP) measurements. The results highlight significant turbulence production and dissipation within the wake, particularly in the upper half of the water column, creating a velocity deficit and enhancing mixing. An analysis revealed that within the wake, the seabed drag coefficient increased from 3.5×10^{-3} to 7.8×10^{-3}, suggesting greater seabed mobility and sediment transport. Eddy viscosity was found to be an order of magnitude higher in the wake, indicating enhanced vertical mixing throughout the water column. [8]

A study by Schultze et al. used large eddy simulations (LES) to model the turbulence and mixing generated by offshore wind farm monopiles in stratified coastal waters. The simulations were conducted using the PALM model, which solves the incompressible Navier-Stokes equations under the Boussinesq approximation. LES explicitly resolved large-scale turbulent eddies, while smaller subgrid-scale turbulence was parameterized. A monopile with a diameter of 7 m was placed in the computational domain. Non-periodic inflow and outflow conditions along the primary flow axis. A precursor simulation with turbulence recycling generated inflow turbulence. Four stratification scenarios, with temperature gradients ranging from 1.5°C/10 m to 3.5°C/10 m, were modeled. [41]

While the destratification effects of conventional monopiles are already looked into, the potential for perforations to mitigate these effects remains unexplored.

1.2.4. Perforated Monopile Designs

Perforated monopile designs have been proposed as a means to mitigate wave loads and potentially reduce the environmental impact of monopile foundations. The study "Wave Load Mitigation by Perforation of Monopiles" by Andersen et. al (2020) assesses the mitigation of wave loads on a monopile by perforation of the shell. The perforation design consists of elliptical holes in the vicinity of the splash zone. Wave loads are estimated for both regular and irregular waves through physical model tests in a wave flume. The study finds that load reductions in the order of 6%–20% are achievable, demonstrating the potential to reduce fatigue wave loads. [4]

1.3. Gap in the Literature

While there is substantial numerical and physical research on the structural design and environmental impacts of monopile foundations, there are no studies assessing the wake effects of perforated monopile designs. This also means that the comparison of the effects of regular and perforated monopile designs on sea water stratification has not been made. This gap highlights the need for further investigation into how different monopile designs influence vertical mixing and stratification.

1.4. Research Problem

In regions like the Mid-Atlantic Bight, seasonal thermoclines are critical for sustaining marine ecosystems. The thermocline, a sharp vertical gradient in temperature, separates warmer surface waters from

a colder bottom layer. This natural stratification is said to be essential for maintaining the balance of marine ecosystems and supporting biodiversity, as stated in subsection 1.1.4

Offshore wind turbine monopiles introduce anthropogenic vertical mixing to the water column by creating turbulent wakes downstream of their foundations. These wakes disrupt the natural stratification of the water column, which is called destratification, as demonstrated by Austin et. al [8]. The destratification of the water column could have significant ecological consequences.

To address these ecological concerns, the concept of perforated monopiles has been proposed as a potential mitigation strategy. By allowing water to flow more freely through the monopile, perforations may reduce the turbulence and wake-induced mixing that leads to destratification. However, the effectiveness of perforated monopiles in preserving stratification in seasonally stratified waters has not been studied, as can be red in section 1.2.

1.5. Research objective

This study aims to assess the potential of perforated monopiles to mitigate seawater destratification compared to conventional designs. By examining their influence on turbulence, vertical mixing, and thermal stratification, the research seeks to determine whether perforations can effectively preserve ocean stratification. The outcomes of this research will contribute to understanding the spatial extent of monopile-induced destratification and evaluate the feasibility of perforated monopiles as a mitigation strategy. Besides that, this study aims to provide recommendations for alternatively designing offshore wind farms to minimize ecological impacts while supporting renewable energy goals.

1.6. Research Scope

This research focuses on the impact of offshore wind turbine monopile foundations on ocean stratification, specifically comparing regular and perforated monopile designs. The scope of this study is defined by the following key considerations:

Single Monopile Analysis: The study investigates the effects of a single monopile on seawater destratification rather than assessing a full wind farm environment. This isolated approach allows for a more controlled analysis of the flow dynamics around monopiles without additional external interactions. Besides that, it is more computationally feasible to implement this approach, since for simulating several turbines, a larger grid would be required.

Steady Flow Conditions: A steady inflow velocity is assumed for all computational simulations, meaning transient or time-dependent effects of tidal variations and fluctuating currents are not explicitly modeled.

Homogeneous Salinity Assumption: The study assumes that there are no differences in salinity in the water column and with that it does not contribute to stratification changes, as it has no influence on the buoyancy forces. This simplification allows the research to focus solely on temperature stratification.

1.7. Research Questions

This study aims to assess how perforated monopiles influence ocean stratification compared to conventional monopiles through answering the following research questions:

1.7.1. Main research question

How do perforated monopile designs influence seawater stratification when compared to regular monopiles?

1.7.2. Supporting research questions

1. *What hydrodynamic mechanisms contribute to the destratification of seawater caused by monopiles, and how does a perforated design influence these mechanisms?*
   Answering this question involves analyzing key hydrodynamic processes such as turbulence generation, wake formation, and vertical mixing to explain destratification processes at play.
2. *How does initial stratification strength influence destratification rates for regular and perforated monopiles?*

This question assesses the sensitivity of stratification breakdown to varying initial conditions, which is critical for evaluating the effectiveness of perforated designs under different environmental conditions.

By addressing these questions, the research aims to provide insights into the effectiveness of perforated monopiles in reducing destratification, contributing to the sustainable development of offshore wind energy infrastructure.

2
Theoretical Background

This section dives into the theoretical background of this research. The goal of this section is to provide and overview of the numerical side of this work.

2.1. Navier-Stokes Equations

Fluid motion is governed by the Navier-Stokes equations, which describe how velocity, pressure, and temperature interact within a fluid. The Navier-Stokes momentum equations are based on three main fundamental physical principles:

1. Conservation of mass (continuity).
2. Conservation of momentum (Newton's second law of Motion): $\boldsymbol{F} = \frac{d}{dt}(m\boldsymbol{u})$.
3. Conservation of Energy.

Below, the equations for incompressible flows are presented:

$$\begin{gathered} \nabla \cdot \mathbf{u} = 0 \\ \frac{\partial \mathbf{u}}{\partial t} + (\mathbf{u} \cdot \nabla)\mathbf{u} = -\frac{1}{\rho}\nabla p + \nu \nabla^2 \mathbf{u} + \mathbf{f} \\ \frac{\partial T}{\partial t} + \mathbf{u} \cdot \nabla T = k \nabla^2 T \end{gathered} \tag{2.1}$$

Where:

- ρ = material density $[\frac{kg}{m^3}]$
- ∇ = nabla operator
- $\mathbf{u}$ = velocity component $[\frac{m}{s}]$
- p = pressure $[\frac{kg}{ms^2}]$
- $\nu = \mu/\rho$ = Kinematic viscosity $[\frac{m^2}{s}]$
- k = thermal conductivity $[\frac{W}{mK}]$
- T = Temperature [K]

For water (and most liquids), the incompressibility assumption is valid because its density remains nearly constant under typical flow conditions. This assumption simplifies the Navier-Stokes equations significantly. This simplification reduces the computational load in computational fluid dynamics.

2.2. The Boussinesq Approximation

The Boussinesq approximation simplifies the incompressible Navier-Stokes equations for flows where density variations are small but play a significant role in buoyancy effects. The key idea is to assume that density differences are negligible everywhere except in the buoyancy term, where they drive motion due to gravity [29]. The Boussinesq approximated Navier-Stokes equations are stated below.

$$\begin{gathered}\nabla \cdot \mathbf{u} = 0 \\ \frac{\partial \mathbf{u}}{\partial t} + (\mathbf{u} \cdot \nabla)\mathbf{u} = -\frac{1}{\rho_0}\nabla p + \nu \nabla^2 \mathbf{u} + \mathbf{g}\beta(T - T_0) \\ \frac{\partial T}{\partial t} + (\mathbf{u} \cdot \nabla)T = \alpha \nabla^2 T\end{gathered} \tag{2.2}$$

Where:

- ρ_0 = Reference density $[\frac{kg}{m^3}]$
- β = Thermal expansion coefficient $[K^{-1}]$
- T = Local temperature [K]
- T_0 = Reference temperature [K]

The Boussinesq approximation holds well for simulating thermal stratification in the ocean because density differences, due to the vertical temperature profile, are small but significant enough to affect buoyancy. As observed from Equation 2.2, the density decreases for higher temperature, leading to a reduced downward force through the downward pointing vector **g**.

2.2.1. The Boundary Layer / Law of the Wall

In fluid dynamics, walls are a source of turbulence, leading to complex flow patterns. In 1905, Prandtl introduced the boundary layer. It is stated that at the boundary layer, the velocity of the fluid is equal to zero [7]. This is called the no-slip condition, which states that the speed of the fluid at the wall must match the speed of the boundary wall, so there is no relative motion between the fluid and the solid surface [2]. The flow within the boundary layer is influenced by the friction coming from the wall. This boundary layer needs to be resolved in CFD. Von Kármán was the first one to publish on this subject [43]; he stated that the average velocity of a turbulent flow is proportional to the logarithm of the distance to the wall. In CFD, this concept is applied to parts of the flow that are near a wall. In the law of the wall, the boundary layer is split up into three main parts, which can ben seen in Figure 2.1:

1. Viscous Sublayer (closest to the wall).
    - In this layer, the flow is dominated by viscous forces and turbulence is minimal.
    - The flow velocity is approximately linear with respect to the distance from the wall.
2. Buffer Layer.
    - In this layer, both viscous and turbulent effects play a role.
    - The velocity profile starts transitioning from linear to logarithmic.
3. Logarithmic (Log) Layer (further from the wall).
    - The turbulent effects dominate in this regions, and the velocity profile follows a logarithmic distribution.

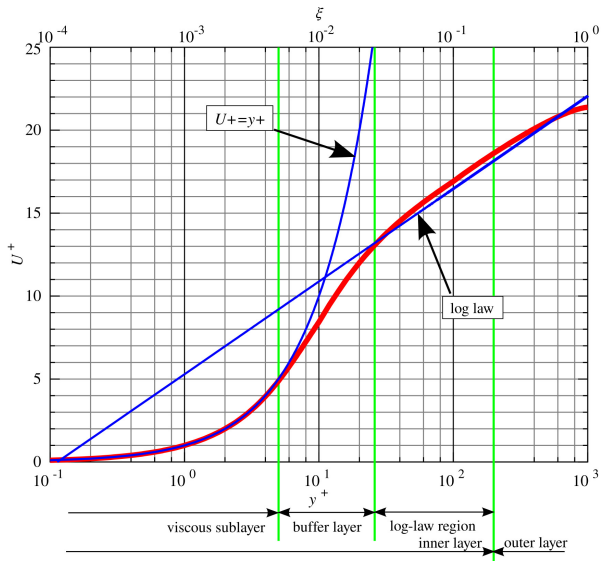

Figure 2.1: Different layers within the boundary layer, divided by green vertical lines, [21]

Numerical modeling of the boundary layer
When performing LES or DNS, a full resolution of the boundary layer is needed to be able to resolve the wall effects. However, when RANS is applied, wall models are used to artificially reconstruct the behavior of the fluid within the turbulent boundary layer.

2.3. Numerical Approaches

Turbulent flows involve a wide range of scales, from large energy-containing eddies to small dissipative scales. Resolving all these scales directly (as in Direct Numerical Simulation, DNS) is computationally expensive. Therefore, models like Large Eddy Simulation (LES) and Reynolds-Averaged Navier-Stokes (RANS) are used to approximate the effects of smaller scales. This means that within the domain of CFD, there are three main types of accuracy scales for simulating flow of a fluid:

- Direct Numerical Simulation (DNS)
- Large Eddy Simulation (LES)
- Reynolds Averaged Navier-Stokes (RANS)

Figure 2.2 shows the detail of different CFD model approaches compared to each other. The measure of detail means how much of the real physics is resolved.

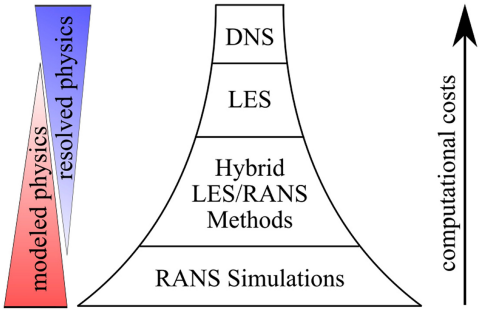

(a) Hierarchy of CFD approaches based on computational costs and amount of resolved details, [53]

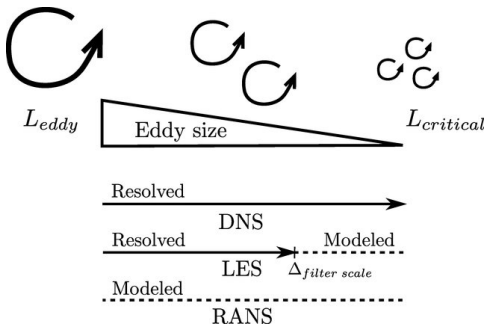

(b) Comparison of different CFD approaches, showing their amount of detail they resolve, [11]

Figure 2.2: Different CFD models approaches and their resolving scale

2.3.1. Direct Numerical Simulation

The DNS approach finds a solutions for the Navier-Stokes equations on all physical scales. To be able to cover all these scales, a very fine spatial domain and small time steps must be used in DN simulations. To cover the spatial scales the domain may be as small as 30 to 100 μm in fluids with a low viscosity such as water. The required timescale to cover the detailed region of the energy spectrum gets smaller for higher Reynolds number, as the fluctuation frequency increases for higher Reynolds numbers. It can be stated that with currently available computational power, DNS can only be applied to low to moderately turbulent flows [15].

Kolmogorov Microscales

The smallest scaled that are resolved by DNS are referred to as the Kolmogorov microscales, denoted by η. This scale is the smallest dimension of eddies encountered in a turbulent flow and is defined as follows [27]:

$$\eta = (\frac{\nu^3}{\varepsilon})^{\frac{1}{4}} \tag{2.3}$$

Where:

- ε= Average rate of dissipation of TKE per unit mass

2.3.2. Large Eddy Simulation

With LES, only the large scales of turbulence are resolved. The Kolmogorov microscales or viscosity dominated scales and part of the inertial range are modeled to reduce computational cost compared to DNS. The Idea behind LES is that large scale turbulence is different for each problem, but the smaller scales are more universal and isotropic [24].

2.3.3. Reynolds-Averaged Navier-Stokes

A method for approximating turbulent flow is by decomposing flow variables into a mean part and a fluctuating part. This decomposition allows engineers and scientists to focus on modeling the average behavior of the flow, rather than the complex and unpredictable instantaneous fluctuations in a turbulent flow. This process is called Reynolds decomposition, and is illustrated in Figure 2.3.

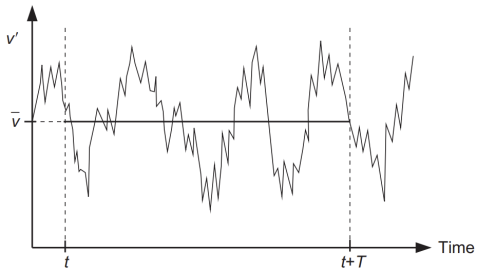

Figure 2.3: Reynolds averaging, illustrating the fluctuating part of the turbulence u' and the mean $\overline{u}$, [10]

Applying time averaging to the incompressible Navier-stokes equations Equation 2.1, the Reynolds-averaged Navier Stokes equations for the conservation of mass and momentum are obtained.

$$\begin{gathered} \nabla \cdot \overline{\mathbf{u}} = 0 \\ \frac{\partial \rho \overline{\mathbf{u}}}{\partial t} + \nabla \rho \overline{\mathbf{u}\mathbf{u}} = -\nabla \overline{p} + \mu \nabla^2 \overline{\mathbf{u}} - \nabla \rho \overline{\mathbf{u}'\mathbf{u}'} \end{gathered} \tag{2.4}$$

Where:

- μ = Dynamic viscosity $[\frac{kg}{ms}]$
- $\mathbf{u}'$ = Fluctuating velocity component (from Reynolds decomposition)

- $\overline{\mathbf{u}'\mathbf{u}'}$ = Reynolds-stress tensor

Reynolds stress
Applying Reynolds decomposition to the Navier-Stokes equations gives rise to the Reynolds stresses. They are called ”stresses” because they represent momentum transfer due to turbulence, having a diffusive nature as they contribute to the turbulent transport of momentum. However these are not caused by viscous processes in the molecular sense. One should therefore consider the approximation of turbulent stresses by means of a turbulent viscosity as a rather coarse and imperfect approach. Solving for the turbulent fluctuation at all relevant length scales would require a modeling effort that is unfeasible for the large scale as considered in this study. Therefore, a Reynolds averaged approach is taken here. [5]. In simple terms, the closure problem arises because turbulence introduces fluctuating velocity components that cannot be directly solved.

Closure problem
Applying Reynolds averaging to the Navier-Stokes equations poses a problem as the new Reynolds stress contains nine new terms with six unknowns. This averaging process means we now have more unknowns than equations. Without additional information, it is impossible to directly compute these Reynolds stresses from only the mean quantities. This means the system of equations is not closed [6].

2.4. Closure of RANS Equations

There are two general approaches to overcome the closure problem occurring in the RANS equations. These are the Boussinesq Hypothesis and the Reynolds Stress Transport Equation Modeling or Reynolds Stress Modeling (RSM).

2.4.1. The Boussinesq Eddy Viscosity Hypothesis

In 1877, Boussinesq stated that the transfer of momentum from turbulent eddies can be modeled with so-called ’eddy viscosity’, ν_t. It is a way to approximate the Reynolds stresses and express them in terms of the mean flow properties and is a method to close the RANS equations without solving for all turbulent fluctuations directly. The Boussinesq Eddy Viscosity Hypothesis (BEVH) states that the Reynolds stress tensor $\overline{\mathbf{u}'\mathbf{u}'}$ can be written as follows [40] (using Einstein Notation):

$$\overline{u_i' u_j'} = -\nu_t \left(\frac{\partial \overline{u}_i}{\partial x_j} + \frac{\partial \overline{u}_j}{\partial x_i} \right) + \frac{2}{3} k \delta_{ij} \tag{2.5}$$

Where:

- ν_t = Turbulence eddy viscosity or $[\frac{m^2}{s}]$
- $k = \frac{1}{2}\overline{u_i' u_i'}$ = Turbulence kinetic energy
- δ_{ij} = Kronecker delta $(= 0 if i \neq j, = 1 if i = j)$

The eddy viscosity can be considered a constant value, which can work well for less complex flow regimes.

Eddy viscosity turbulence models
There are several models available which use the eddy viscosity hypothesis. These models are called Eddy Viscosity Models (EVMs). These can be divided in the following categories:

- Linear eddy viscosity models
  - Algebraic models
  - One equation models
  - Two equation models

- Nonlinear eddy viscosity models

Eddy viscosity are isotropic turbulence models. Two-equation turbulence models, such as the k-epsilon and k-omega models, are among the most widely used in engineering. These models have become industry standards due to their applicability to a variety of engineering problems. These two models can also be combined through the k-omega SST model, where SST stands for Shear Stress Transport. The reason for combining these turbulence models is that k-omega model performs well in the boundary layer region whereas k-epsilon model shows more accurate results in the free stream region of the flow, see Figure 2.4. The SST model blends the k-omega and the k-epsilon models using a blending function, using a weighting function based on the distance from the wall.

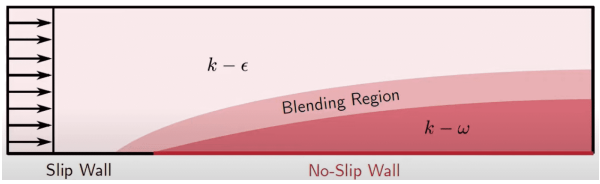

Figure 2.4: k-omega SST models, a combination between the turbulence models k-epsilon and k-omega, [22]

For the K-omega-SST model, the turbulent eddy viscosity is calculated as follows:

$$\nu_t = \frac{a_1 k}{\max(a_1 \omega, SF_2)} \tag{2.6}$$

where:

- ν_t = turbulent eddy viscosity (m^2/s)
- k = turbulent kinetic energy (m^2/s^2)
- ω = specific dissipation rate (s^{-1})
- S = strain rate magnitude (s^{-1})
- a_1 = empirical model constant ($a_1 = 0.31$)
- F_2 = blending function that controls the transition between near-wall and free-shear behavior

2.4.2. Reynolds Stress Model

Reynolds Stress Models (RSMs) avoid the eddy viscosity approach by directly computing the individual components of the Reynolds stress tensor using the exact Reynolds stress transport equation. This allows RSMs to capture complex interactions in turbulent flow fields, including the directional effects of Reynolds stresses. In contrast, isotropic eddy-viscosity models like the k-epsilon and k-omega models have notable limitations in handling complex, real-life turbulent flows often encountered in engineering. These limitations become particularly obvious when dealing with flows with for example significant streamline curvature or with recirculation zones. A downside of RSMs is that they are computationally more expensive than EVMs. [13]

2.5. Spatial Discretization

The numerical solution to the Navier-Stokes equations can be found by three classical discretization methods: the Finite Difference Method (FDM), Finite Element Method (FEM) and the Finite Volume Method (FVM). [36]

The Finite Volume Method (FVM) is ideal for CFD because it ensures conservation of mass, momentum, and energy within each control volume, which is crucial for accurate fluid flow simulations. Unlike the Finite Element Method (FEM), which can be computationally expensive and complex, FVM handles complex geometries and boundary conditions more efficiently. Compared to the Finite Difference Method (FDM), FVM is more flexible with unstructured meshes and better suited for practical engineering problems. Overall, FVM's robustness, stability, and ease of implementation make it a preferred

choice for CFD. It's widely used in industry and research for modeling ocean currents, offshore structures, and wave interactions.

2.5.1. Finite Volume Method

For the FVM, the spatial domain is divided into a finite number of control volumes (grid cells). Each cell represents a discrete portion of the domain. One of these finite volumes is represented in Figure 2.5

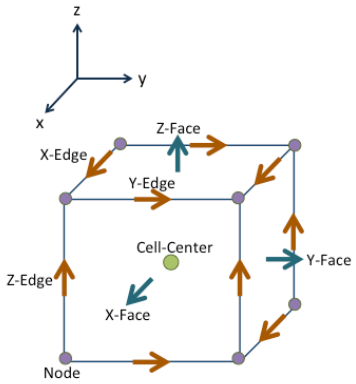

Figure 2.5: One grid cell, showing the cell-center and the different faces [19]

Each cell is assigned an initial condition and at the boundaries of the domain, boundary conditions are set. When needed, sources and sinks on specific locations in the domain can be set. When a simulation is started, the values at the faces are obtained by interpolating between centroid values. There are many interpolation schemes available, with different applications, such as the time differentiation schemes, gradient schemes and more. A few examples are listed below:

1. Gauss linear
2. Least squares
3. Linear upwind

The Navier-Stokes equations are integrated over the volume of each cell. After this, the divergence theorem or 'Gauss theorem' is applied. Simplified, the divergence theorem states that the volume integral of a continuously differentiable vector field can be related to the surface integral, see the equation below. [34]

$$\iiint_V (\nabla \cdot \mathbf{F}) \mathrm{d}V = \oiint_S (\mathbf{F} \cdot \hat{\mathbf{n}}) \mathrm{d}S \tag{2.7}$$

The previously obtained face values are then plugged into the discrete form of the Navier-Stokes equations are the faces to calculate the flux going through the face. These face fluxes are then used to obtain the cell-centroid value for each grid cell. This process is repeated until convergence is reached. Like FDM, FVM can make use of a non-equispaced mesh or unstructured mesh, meaning it is possible to capture higher resolutions at specific locations. This is commonly applied to capture more information at locations with more complex flow regimes, for example near an obstacle.
The most commonly adopted method for CFD applications is the Finite Volume Method.

2.6. Residuals

Residuals provide measure of how well the discretized governing equations are satisfied during the iterative solution process. They are used to monitor the progress of convergence and ensure that the numerical solution approaches the real solution of the governing equations. The residuals are defined as follows:

$$\mathbf{r} = \mathbf{A}\mathbf{x} - \mathbf{b} \tag{2.8}$$

The residuals in each grid cell are expressed into a global residual to obtain an idea of how well the entire domain is converged. For steady-state simulations, the simulation is considered converged when

the residuals fall below a certain threshold value, for example 10^{-6}. Figure 2.6 shows and example of the decay of the residuals in a steady-state OpenFOAM run.

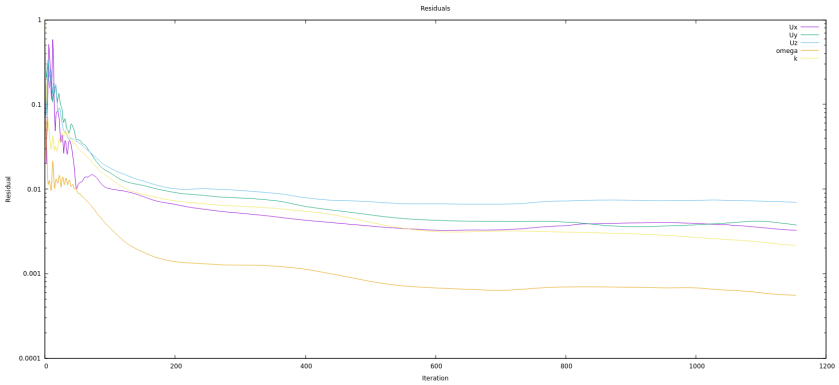

Figure 2.6: Residuals from an OpenFOAM simulation, excluding pressure residuals, plot created using gnuplot

2.7. Initial and Boundary Conditions

Initial and boundary conditions are essential components in CFD simulations as they define the constraints and starting state of the system being modeled. Proper specification of these conditions ensures that the simulation accurately represents the physical problem and converges to meaningful results.

2.7.1. Initial Conditions

Initial conditions are used to specify the initial state of the domain in terms of pressure, velocity, turbulence quantities, temperature and more. For example, the initial velocity field could be set the $0.4\frac{m}{s}$

2.7.2. Boundary Conditions

Boundary conditions define how the flow interacts with the boundaries of the computational domain. Figure 2.7 shows a basic computational domain with the Ahmed body inside. In this case the domain would have 7 boundary conditions:

1. Inlet
2. Outlet
3. Bottom (wall)
4. Top
5. Front
6. Back
7. Monopile (wall)

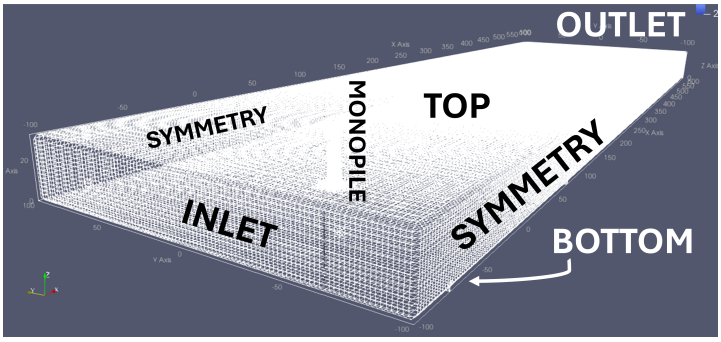

Figure 2.7: Boundary conditions on a rectangular computational domain, with a monopile cylinder inside

There are numerous types of boundary conditions. Each boundary can have a type and value for different physical quantities, such as velocity, pressure, temperature, turbulence, salinity, viscosity and more. A few examples are listed below for the velocity, pressure and turbulence on 3 boundaries, where on the left the physical quantity and on the right the type of boundary condition are mentioned:

Inlet Boundary

- Velocity fixedValue
- Pressure totalPressure
- Turbulence fixedValue (for k and ω)

Outlet Boundary

- Velocity ZeroGradient
- Pressure fixedValue
- Turbulence zeroGradient

Object Boundary

- Velocity noSlip
- Pressure fixedFluxPressure
- Turbulence kqRWallFunction

2.8. Solution Algorithms

As the governing equations (Navier-Stokes equations) are nonlinear and coupled, they require numerical techniques to be solved. The solution algorithm or ”solver” determines how the equations are discretized subsection 2.5.1 and how the systems are iteratively solved. Within OpenFOAM, there’s numerous different solver available, with different specific features. A few are stated below:

- Incompressible Flow Solvers: simpleFoam, icoFoam, pimpleFoam
- Compressible Flow Solvers: rhoCentralFoam, sonicFoam, rhoPimpleFoam
- Multiphase Flow Solvers: interFoam, bubbleFoam
- Buoyancy-Driven Flow Solvers: BuoyantBoussinesqPimpleFoam, BuoyantBoussinesqSimpleFoam

2.9. Steady-State or Transient

CFD simulations can be classified into transient and steady-state simulations based on the time dependence of the governing equations and the behavior of the flow being analyzed. This distinction is

fundamental in CFD, as it determines the approach used to solve the flow equations and the type of results obtained.

Steady-State Simulations In Steady-State simulations, the flow properties (f.e. velocity, pressure and temperature) are considered constant with respect to time and in the governing equations the following assumption is applied:

$$\frac{\partial}{\partial t}(\cdot) = 0 \tag{2.9}$$

Where $\cdot$ = some flow property This means that there is no time-dependent behavior. This means that the system iterates until it reaches equilibrium and all transient behavior is gone or at least negligible. It is only applicable to CFD simulations without transient phenomena, so only applicable to steady or quasi-steady problems.

Transient Simulations In a transient simulation, the flow properties vary with time, and the governing equations include the time-dependent term:

$$\frac{\partial}{\partial t}(\cdot) \neq 0 \tag{2.10}$$

This allows for the capturing of the change of flow over time in a simulation. It is applied in simulations with oscillatory flows, vortex shedding, dynamic boundary conditions like time-varying inflow or thermal loads. The downside is that it is more computationally expensive than steady-state simulations. [49]

2.10. Parameter Under-Relaxation

Parameter under-relaxation is a numerical technique used in iterative solvers to improve the convergence and stability of the solution process. It involves modifying the update step of a variable or equation during an iterative process by applying a scaling factor α, known as the relaxation factor, to control the extent of changes made at each iteration. For under-relaxation, the value of α should be between 0 and 1. Figure 2.8 is an example of this process, where the calculated value for T, T_{calc}, is multiplied by α in order to arrive at a reduced value for T.

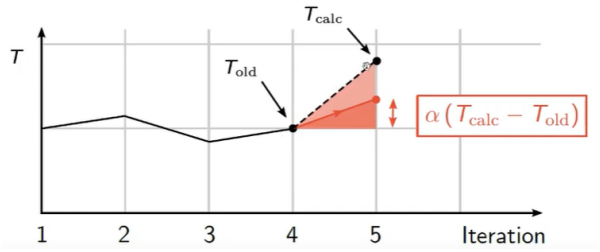

Figure 2.8: Parameter under relaxation, [20]

2.11. OpenFOAM

To wrap up this dive into CFD, it is fitting to shed light on OpenFOAM (Open Field Operation and Manipulation), which one of the most powerful CFD software frameworks available today. OpenFOAM is an open-source C++ toolbox which can be used to simulate a large range of fluid dynamics problems. It can be used for both research and engineering application because of its adaptability, transparency, and extensive capabilities. OpenFOAM combines all the information stated above into the toolbox.

3
Methodology

This chapter provides the framework for answering the research objectives, ensuring a clear connection between the methodology and the research problem. By going into the computational setup, assumptions, and analysis techniques, it ensures the reproducibility and credibility of the study's findings. The methodology begins with the definition of the computational domain, followed by the setup of boundary conditions, grid design, and simulation parameters. Also, the setup of the different cases and scenarios are shown. Validation of the numerical model is conducted where applicable, and sensitivity analyses are performed to ensure robustness in the results.

3.1. Model Choice

3.1.1. OpenFOAM

OpenFOAM was selected as the CFD software for this study due to its flexibility, suitability for simulating complex fluid dynamics and because it is free. Unlike software such as ANSYS Fluent or COMSOL, OpenFOAM is open-source, allowing for full freedom and for insight into the code. Besides that, OpenFOAM's active community and extensive documentation provide strong support for users, ensuring that challenges encountered during the study can be tackled quickly, without significantly delaying the process.

3.1.2. RANS

As described in section 2.3, there are three main numerical approaches. Reynolds Averaged Navier Stokes was chosen for this thesis because it offers a practical yet sufficiently accurate approach for modeling offshore monopile-induced flow structures while ensuring computational feasibility. This is because the domain is large and requires high computational power. Moving towards LES would require even more computational power.

3.1.3. Turbulence Model

This research makes use of the k-omega SST turbulence model. As described in section 2.4,two-equation turbulence models are the most widely adopted turbulence models nowadays. As the k-omega SST model combines the k-omega and the k-epsilon models, using a blending region, as can be seen in Figure 2.4, it exploits the model advantages, particularly suited for developing and separating flows, in both the near-wall region as in the free-stream region.

3.1.4. Wall Models

As the scale of the problem in this research is large, as described in section 3.2, it is too computationally expensive to properly resolve the boundary layer. For that reason, wall models are used for the near-wall treatment of the flow physics. This allows for lower values of y^+, as described in subsection 2.2.1. The wall models used in this research are the following:

Parameter	Wall Model
Turbulence Kinetic Energy k	kqRWallFunction
Specific TKE dissipation rate ω	omegaWallFunction
Turbulent Eddy Viscosity ν_t	nutUWallFunction
Turbulent Thermal Diffusivity α_t	alphatJayatillekeWallFunction (Pr_t = 0.85)

Table 3.1: Wall models used in this research

3.2. Computational Domain and Grid

3.2.1. Dimensions

Table 3.2 shows the dimensions of the computational domain in this research. The inflow is always in x-direction. The z-dimensions is in vertical direction, so it ranges from the seafloor until the waterline.

Direction	Distance [m]
x	1100
y	200
z (vertical)	32

Table 3.2: Dimensions of the Computational Domain

A top view of the computational domain is displayed in Figure 3.1. The monopile is always situated at x = 0 and y = 0, being represented by the white hole in the domain. The flow direction is from left to right.

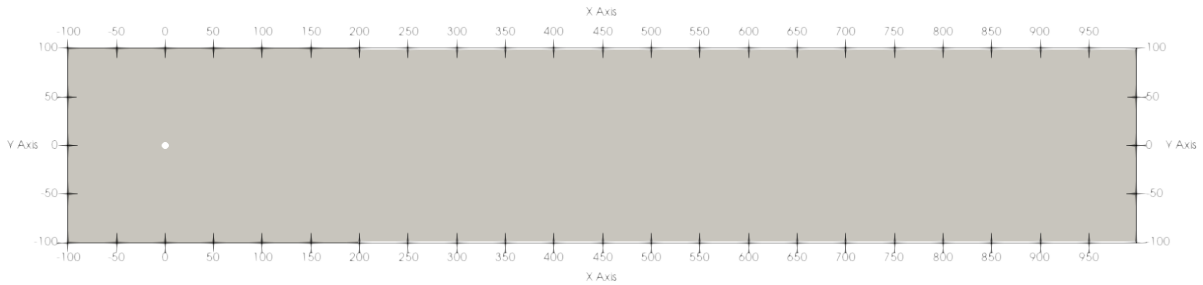

Figure 3.1: Top view of the computational domain, with the white hole representing the monopile

3.2.2. Initial Conditions

To properly initialize each simulation, it important to set the right initial conditions. A few initial conditions are stated in Table 3.3, below:

Condition	Magnitude
T($0 \leq y \leq 25$)	Dependent on simulation
T($(25 < y \leq 32)$	284.75 K
U(x, y, z)	(0.4, 0, 0) m/s

Table 3.3: Initial conditions

Figure 3.2 shows a side view of the domain, where it can be observed that the bottom layer (0 - 25 m) corresponds to 284.25 K and the top layer (25 - 32 m) corresponds to 287.85 K. This corresponds to an initial stratification of 3.5 K.

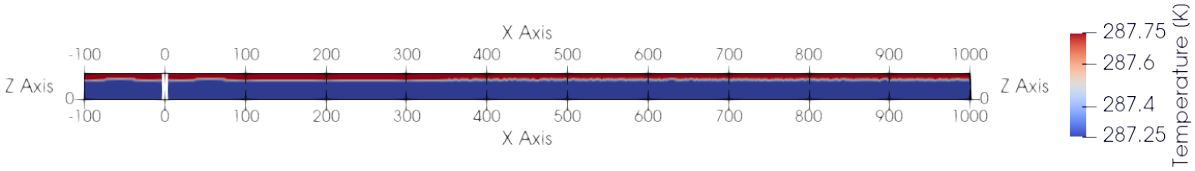

Figure 3.2: Side view of the domain with the initialized temperature

3.2.3. Boundary Conditions

Figure 3.3 shows the boundaries of the computational domain in this research. The sides are subjected to a symmetry boundary condition. For the computations, the inlet boundary is split into two parts, ranging from 0 to 25 m and from 25 to 32 m, as shown in Figure 3.2, which are called inletBot and inletTop.

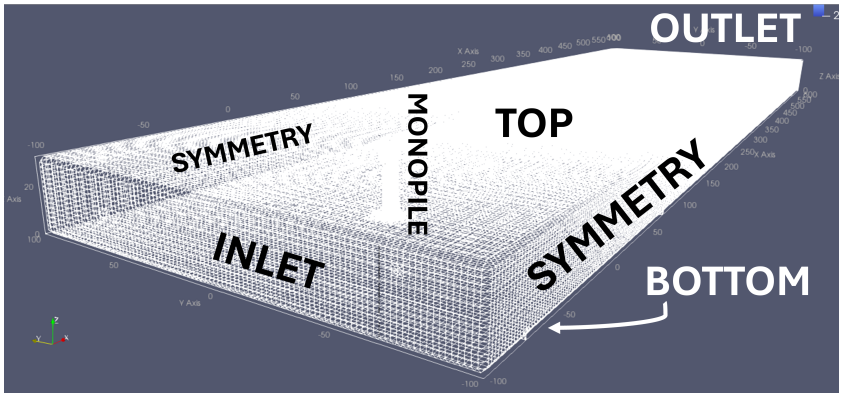

Figure 3.3: Boundaries of the computational domain

Table Table 3.4 shows some of the boundary condition types included in the models.

	T	U	p_rgh
InletBot	fixedValue	fixedValue	zeroGradient
InletTop	fixedValue	fixedValue	zeroGradient
Bottom	zeroGradient	noSlip	zeroGradient
Top	zeroGradient	zeroGradient	zeroGradient
Symmetry	symmetry	symmetry	symmetry
Monopile	zeroGradient	noSlip	fixedFluxPressure
Outlet	zeroGradient	zeroGradient	zeroGradient

Table 3.4: Boundary Conditions for T, U and pressure. Excluding k, omega, alphat and nut

3.3. Cases & Scenarios

3.3.1. Cases

In this research, the set-up of the domain is referred to as a case. This means that different monopile designs are referred to as different cases. The three cases in this research are stated below.

Base Case

The base case represents the case with a regular monopile in the computational domain. An illustration of this monopile is provided in Figure 3.4.

The monopile has a diameter of 7 m and extends 32 m in height, matching the water column depth. This diameter was initially selected based on a study by Schultze et al. [41] to facilitate a potential comparison. However, as the study progressed, it was determined that direct validation against this reference was not feasible.

Despite this, the 7 m diameter was held on to as it represents a realistic industry-standard size commonly used in modern offshore wind farms. This ensures that the findings remain relevant for real-world applications while maintaining computational feasibility.

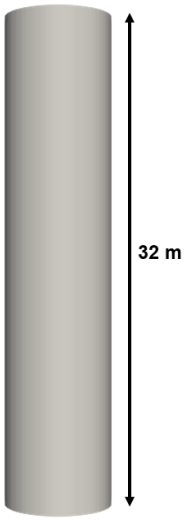

Figure 3.4: Regular monopile used in this research, including dimensions

Perforated Monopile Case
The perforated monopile case features a perforated monopile within the computational domain. This design is an adaptation of the perforated monopile illustrated in Figure 1.6, as presented by Andersen et al. [4].

In the study by Andersen et al., a 10-meter diameter perforated monopile was used. For this research, the design has been scaled down to a 7-meter diameter to be consistent with the base case. Accordingly, the perforation dimensions have been scaled proportionally by a factor of $\frac{7}{10} = 0.7$ to preserve the relative structural characteristics.

Similar to the base case, the monopile extends 32 meters in height, aligning with the water depth in the domain. A 3D illustration of the adapted perforated monopile is provided in Figure 3.5. The perforations extend from the waterline down to a depth of 9.75 meters.

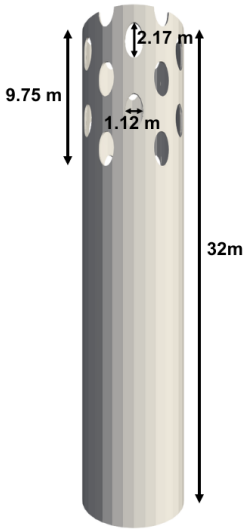

Figure 3.5: Perforated monopile used in this research, including dimensions

3.3.2. Scenarios

To be able to assess the effect of different initial stratification strengths ΔT on the destratification behavior and to be able to validate the research to existing research, the simulations are subjected to several different environmental conditions, called scenarios. The four different scenarios in this research are stated below:

- ΔT = 0.5 K
- ΔT = 1.5 K
- ΔT = 2.5 K
- ΔT = 3.5 K

3.3.3. Refinement Strategies

To be able to capture enough information in places where more complex flow patterns are expected, the initial, castellated mesh, created by the blockMesh utility is refined with the OpenFOAM SnappyHexMesh utility. The the area around and inside the monopile is refined as observed in Figure 3.6. For the regular monopile, the grid is not refined inside the cylinder, as there is no flow inside.

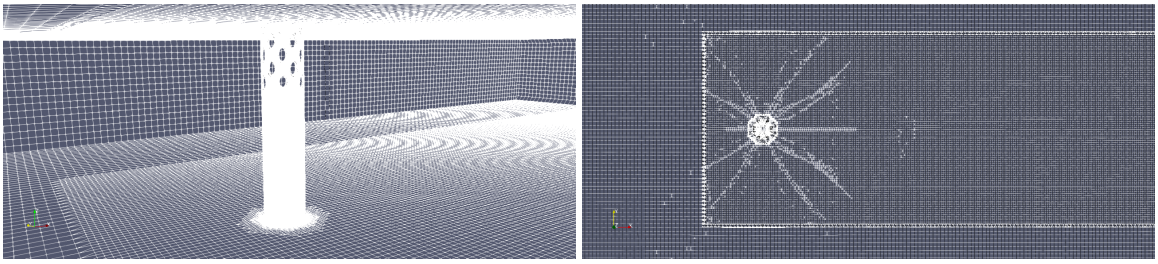

(a) Grid inside view (b) Top view grid

Figure 3.6: Computational grid for the perforated monopile, showing the refinement around the monopile

3.4. Analysis Methods

The results are analyzed and prepared for comparison through four frameworks:

1. Velocity Wake
2. Transverse Flow Profiles
3. Turbulence Parameters
4. Relative Destratification

3.4.1. Velocity Wake

To analyze the flow behavior around the different monopile designs, velocity distributions are examined at key locations: upstream, within, around, and downstream of the monopiles. Particular focus is placed on the wake region, where flow recovery is assessed.

Velocity wakes are evaluated by comparing local flow velocities to the free-stream velocity. In this study, wake recovery distance is defined as the downstream location where velocity reaches 90% of the free-stream velocity. This threshold is based on the criterion established by Ebdon et al. [16]. While the wake is not yet fully recovered at this point, it is approaching background conditions, making it a practical benchmark for comparison.

Additionally, localized flow behavior near the monopiles is analyzed in detail, with particular attention to the internal flow dynamics within the perforated monopile. This assessment provides insights into how perforations influence wake development and flow reattachment.

3.4.2. Transverse Flow Profiles

The y- and z-components of the flow are analyzed by isolating them fully or partly from the main flow direction (x-direction). First, the flow in front of the monopile is assessed through, among others, the downflow. After this, the y-z-directed flow is analyzed 100 m downstream of the monopiles to analyze potential eddies that are captured in the time averaged RANS. These vertical flow profiles help characterize the mixing efficiency of regular and perforated monopiles.

3.4.3. Turbulence Parameters

The turbulence around the monopiles is assessed through the parameters Turbulence Kinetic Energy, Specific Turbulence Dissipation Rate and Turbulent Eddy Viscosity. This research looks into the location of generation of turbulence for both monopile designs and analyses their deficit by plotting the development of the turbulence parameters over downstream direction and by looking at several z-, y-slices of the computational domain.

To quantify turbulence wake behavior, TKE development is analyzed in two key ways:

- Longitudinal turbulence decay: The evolution of turbulence parameters along the downstream direction.
- Planar turbulence distribution: Multiple z-slice top views of the computational domain are assessed to visualize turbulence intensity and spread.

3.4.4. Relative Destratification

Relative Destratification (RD) is a metric used to quantify the extent of destratification at a specific downstream location, relative to the initial stratification. This approach enables the comparison of different cases and scenarios by condensing destratification effects into a single numerical value. This is useful for comparing the different cases and scenarios. To compute the RD, a representative point in the wake is selected as an indicator of temperature change. In this study, the comparison point is chosen at (500, 0, 32) and is compared to an upstream reference point at (-50, 0, 32). The RD metric is defined mathematically as stated below:

$$\begin{aligned} T_{RD} &= T(-50, 0, 32) - T(500, 0, 32) \\ RD &= (\tfrac{T_{RD}}{\Delta T}) \times 100 \end{aligned} \tag{3.1}$$

where:

- T(-50, 0, 32) represents the reference temperature 50 meters upstream
- T(500, 0, 32) is the temperature measured 500 meters downstream
- ΔT represents the initial temperature difference between the top and bottom of the water column

To further illustrate this calculation, Figure 3.7 presents the vertical temperature profiles at three locations: x = -50 m (red), x = 100 m (green), and x = 500 m (blue). The metrics used in RD calculations are highlighted in the figure.

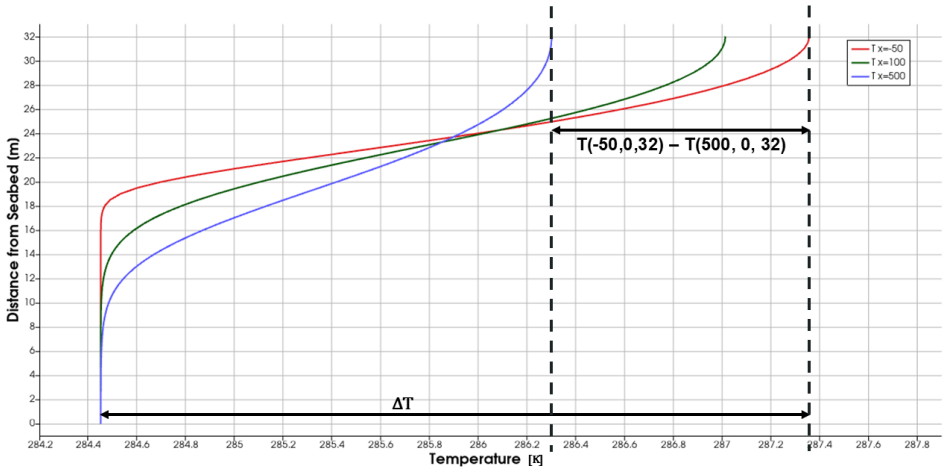

Figure 3.7: Vertical temperature profile at three locations, x = -50 m (red), x = 100 m (green) and x = 500 m (blue). T(-50, 0, 32) - T(500, 0, 32) and ΔT are visualized

3.5. Validation and Verification

To ensure the accuracy and reliability of the computational model, a validation step is performed against existing experimental data. This validation focuses on the turbulence kinetic energy (TKE) in the wake, as turbulence plays a fundamental role in monopile-induced mixing and destratification.

The development of TKE in the wake is compared against experimental measurements from ”The Turbulent Wake of a Monopile Foundation” by Rogan et al. [39]. By benchmarking the numerical results against validated experimental data, this study ensures that the computational model accurately represents key physical processes. The validation method is elaborated in section 4.1.

4
Results

This section presents the key findings of the study, focusing on the hydrodynamic and thermal effects of regular and perforated monopile designs in offshore environments. The results are structured around several critical aspects: velocity wake characteristics, turbulence kinetic energy (TKE) distribution, vertical flow profiles, and the impact on thermal stratification.

The velocity wake analysis examines flow recovery downstream of the monopiles, highlighting the influence of perforations on reducing wake intensity. The turbulence kinetic energy assessment evaluates the extent of mixing induced by monopile-induced turbulence, providing insights into energy dissipation patterns. The vertical flow profiles detail the downflow characteristics in proximity to the monopiles, emphasizing differences in flow structure between regular and perforated designs. Finally, the thermal stratification results assess the relative destratification (RD) induced by each monopile configuration, determining their respective contributions to vertical mixing.

4.1. Model Validation

This section aims to validate the numerical model developed for simulating the turbulent wake of a monopile foundation. The validation is based on comparing the model's predictions with experimental data from the paper "The Turbulent Wake of a Monopile Foundation", [39]. The key parameters used for validation are the Turbulent Kinetic Energy (TKE), the background (free-stream) Turbulent Kinetic Energy (TKE_0), the Relative Excess Turbulence (RET), and the Turbulence Recovery Length scale (TRL).

4.1.1. Validation basis

Relative Excess Turbulence (RET) is the extra turbulence generated by the pile, normalized by the free-stream turbulence. The Turbulence Recovery Length scale (TRL) is the distance downstream (normalized by D) required for RET to fall below a given threshold. The TRL is estimated at 40 for an RET threshold of 1.0 and 400 for an RET threshold of 0.1, according to the research of Rogan et al..
The RET is defined as follows:

$$RET = \frac{TKE - TKE_0}{TKE_0} \tag{4.1}$$

Where:
TKE_0 = Free stream turbulence kinetic energy
TKE = Turbulence Kinetic Energy

The TRL is defined as such:

$$TRL = \frac{x}{D} \tag{4.2}$$

Where:
x = Downstream distance
D = Monopile diameter

From this formula, it follows that, as the monopile diameter in this research is 7 m, the RET thresholds are as follows (Table 4.1):

RET [-]	TRL [m]
1	280
0.1	2800

Table 4.1: RET and TRL for D = 7 m

In the paper from Rogan et al., the experiments are set up in a basin with a depth of 0.50 m. The velocimeters were placed on 0.35 m from the bottom. To acquire a similar scaling, the TKE profile used for this validation is plotted at the following distance from the seabed:

$$z_{plot} = \frac{0.35}{0.50} * 32 = 22.4m \tag{4.3}$$

4.1.2. Validation

Figure 4.1 shows the development from the model in this research over downstream direction. From this figure, distances downstream on which the RET values of 1 and 0.1 are reached are extracted. The free-stream TKE, TKE_0 found, is equal to 2.0e-4 $\frac{m^2}{s^2}$.

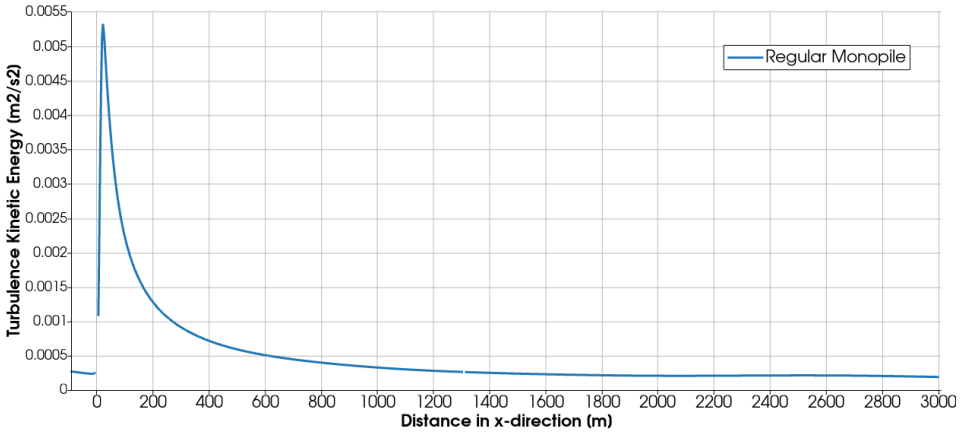

Figure 4.1: Turbulence Kinetic Energy over downstream direction until 3000 m downstream

The values extracted from Figure 4.1 are displayed in Table 4.2. The difference in TRL is +130% and +7%, respectively. This means that in the near wake the model in this research does not match the research by Rogan et al., however, in the far field it seems to match well. The differences could be explained by the different Reynolds numbers, cylinder diameter and other parameters. Besides that, it could be attributed to some modeling inaccuracies.

RET_{Rogan} [-]	TRL_{Rogan} [m]	TRL [m]	Difference [%]
1	280	680	+130
0.1	2800	3000	+7

Table 4.2: RET comparison between [39] and the numerical model in this research

4.2. Velocity Wake

To understand the process of destratification in the wake of the different monopile designs, it is important to understand how the velocity in wake behaves. In this section, the velocity wakes are analyzed and compared. It is important to keep in mind that the model in this research does not include waves, which could have a stabilizing effect on a wake, causing it to reduce into backward conditions earlier.

4.2.1. Regular Monopile

The velocity wake generated by the regular monopile exhibits a clear reduction in velocity magnitude in the immediate downstream region, as observed in Figure 4.7. The velocity profile indicates that the wake recovers gradually as the flow progresses downstream, with the velocity being recovered to 90% of the free-stream velocity after 760 m, indicated by the black horizontal line. In the top view shown in Figure 4.2 it can be observed that the wake becomes wider until a maximum width of 40 m and diminishes over the downstream direction.

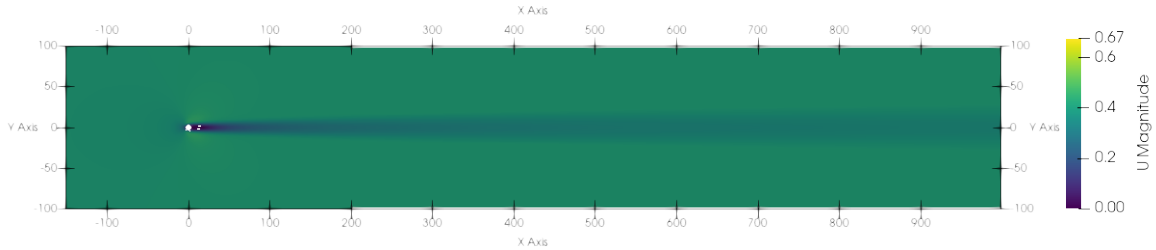

Figure 4.2: Top view of the velocity wake for the Regular monopile, flow direction is rightward, up to 1000 m downstream, values in [m/s]

Figure 4.3 shows the velocity magnitude from a side view through the monopiles center. Reduced velocities are observed over the entire slice, as expected when looking at Figure 4.2. The maximum velocity of 0.67 $\frac{m}{s}$ is caused by the jets flowing through the perforations, which can be seen from Figure 4.5. The maximum velocity for the regular monopile is 0.46 $\frac{m}{s}$, which is the increased flow velocity around the cylinder. Besides that, the boundary layer on the bottom, resulting from the bed friction, is shown by the low velocities near the bed.

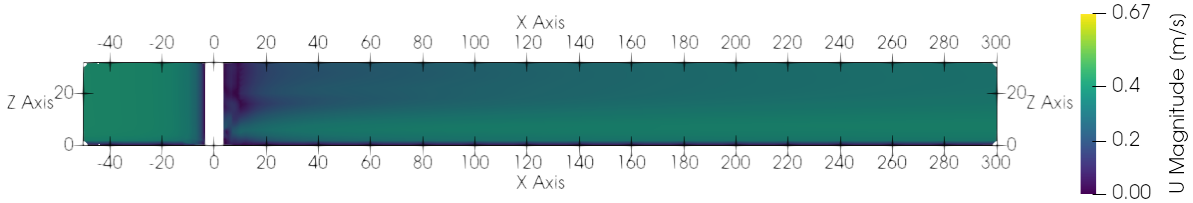

Figure 4.3: Side view of the velocity wake for the Regular monopile through the center of the monopile, flow direction is rightward, slice up to 300 m downstream, values in [m/s]

4.2.2. Perforated Monopile

The perforated monopile demonstrates a rapid velocity recovery downstream. As seen in Figure 4.7, the velocity drops and increases inside the and right behind the monopile in a irregular pattern because of the perforations. The fact that the velocity is recovered to 90% of the free-stream velocity after 210 m suggests that the perforations help with reducing the formation of strong wake recirculation zones, meaning less flow separation.

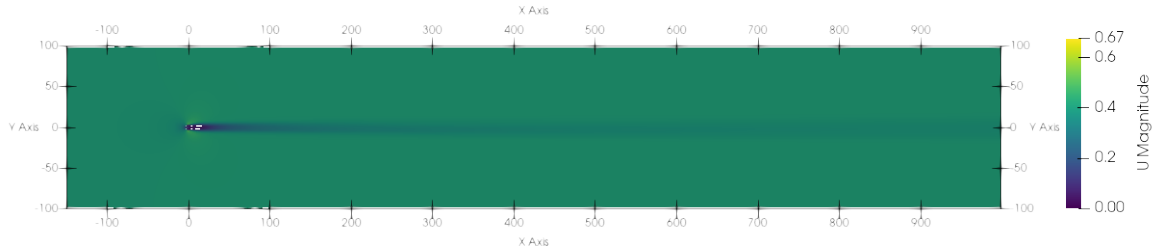

Figure 4.4: Top view of the velocity wake for the Perforated monopile, flow direction is rightward, up to 1000 m downstream, values in [m/s]

From the side profile shown in Figure 4.5, the earlier discussed jets are visible. Due to the flow contraction, the jets maintain a significant velocity.

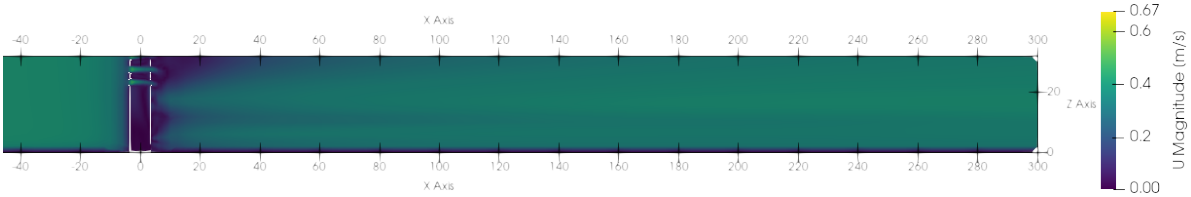

Figure 4.5: Side view of the velocity wake for the Regular monopile, flow direction is rightward, slice up to 300 m downstream, values in [m/s]

Figure 4.6 shows the process of flow separation around a cylinder. For the perforated case, the recirculating flow interacts with the flow through the monopile, depicted by the purple arrow. The flow depicted by the purple arrow accelerates the recirculated flow, reducing the difference in flow velocity between the recirculated part, reducing the amount of separation which in turn reduces the TKE generated.

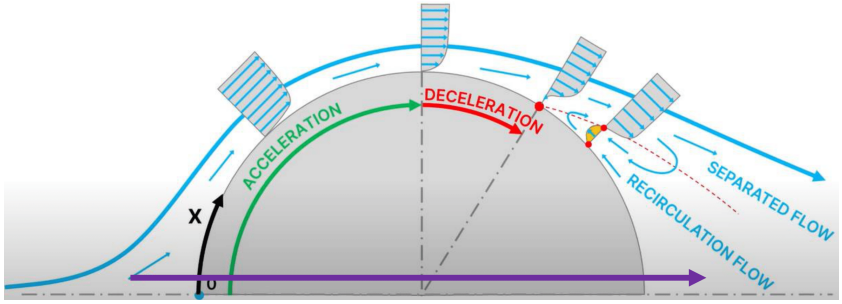

Figure 4.6: Process of flow separation around a cylinder, with the purple arrow (not on scale) depicting the flow through the perforations, figure by [1], edited by author

4.2.3. Velocity Wake Comparison

The comparative velocity wake results, shown in Figure 4.7, highlight differences between the regular and perforated monopile designs. The regular monopile exhibits a more pronounced wake deficit, with lower velocity magnitudes persisting over a longer downstream distance. Conversely, the perforated monopile facilitates a faster velocity recovery and widens less.

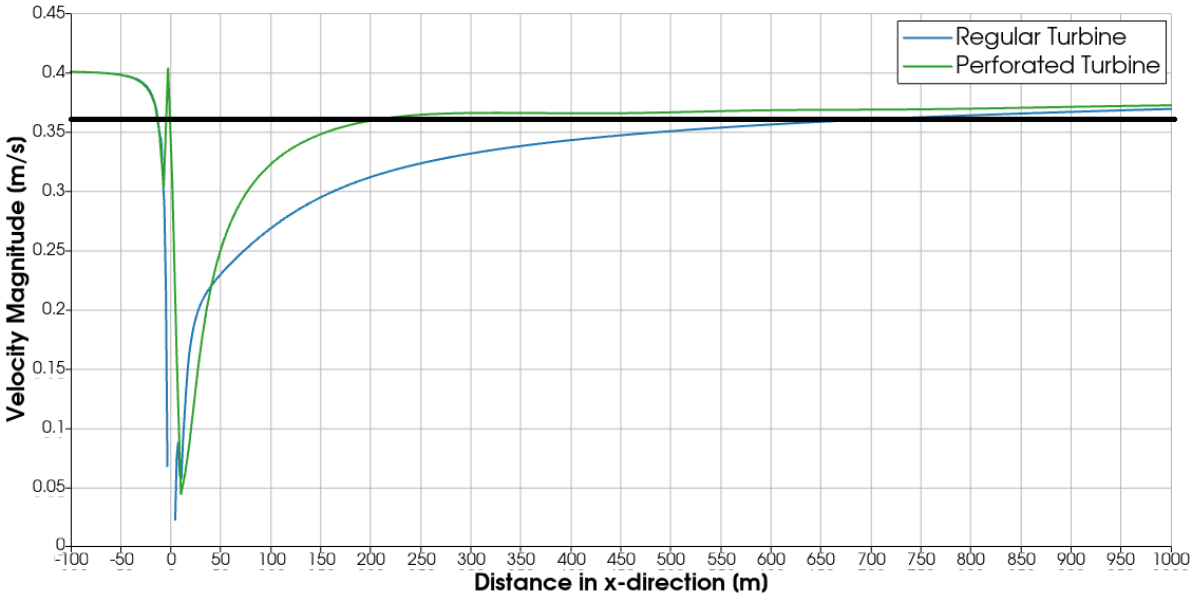

Figure 4.7: Velocity magnitude of the Perforated and Regular monopile of the downstream (x) direction, 0.5 m under the waterline and through the center of the monopile. The black line demonstrates the point where 90% of the free stream velocity is recovered, which is at 660 m downstream for the regular monopile and 210 m downstream for the perforated design

Figure 4.8 shows that the velocity right behind the monopile is higher for the perforated design because of the jets through the pile, interacting with the wake and reducing the flow separation as mentioned before.

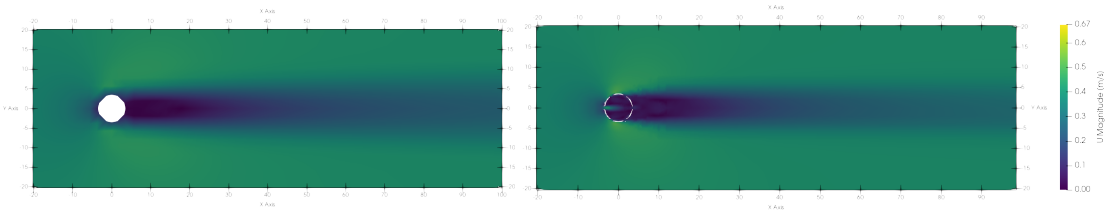

(a) Regular monopile (b) Perforated monopile

Figure 4.8: Close up wake of the regular and perforated monopiles, values in [m/s]

Figure 4.9 illustrates the magnitude of the flow velocity from the upstream side. It is apparent that the boundary layer on the bottom becomes smaller due to the flow acceleration due to contraction around both monopiles. The velocity peaks at 0.67 $\frac{m}{s}$ at the sides of the monopiles, which is 67.5 % higher than the free-stream velocity. This value is in line with other studies [3]. The flow velocity at at the sides of the perforated design stays around the free-stream velocity as flow can pass through the perforations in this region and is thus not forced around the monopile as much as it would normally be.

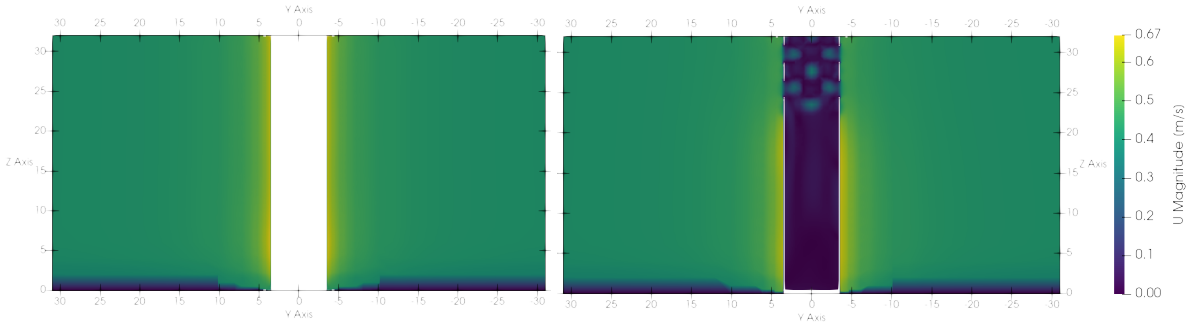

(a) Regular monopile (b) Perforated monopile

Figure 4.9: Front view of the velocity for both monopiles, flow direction into the paper, values in [m/s]

The process of less flow separation occurring for the perforated monopile describes by Figure 4.6 is proven by Figure 4.10. The figure illustrates the how the regular monopile in Figure 4.10a has more inward directed vectors right behind the monopile when compared to the perforated one. The regular monopile exhibits the classical recirculation behind the cylinder, whereas this recirculation is hindered in the case of the perforation design.

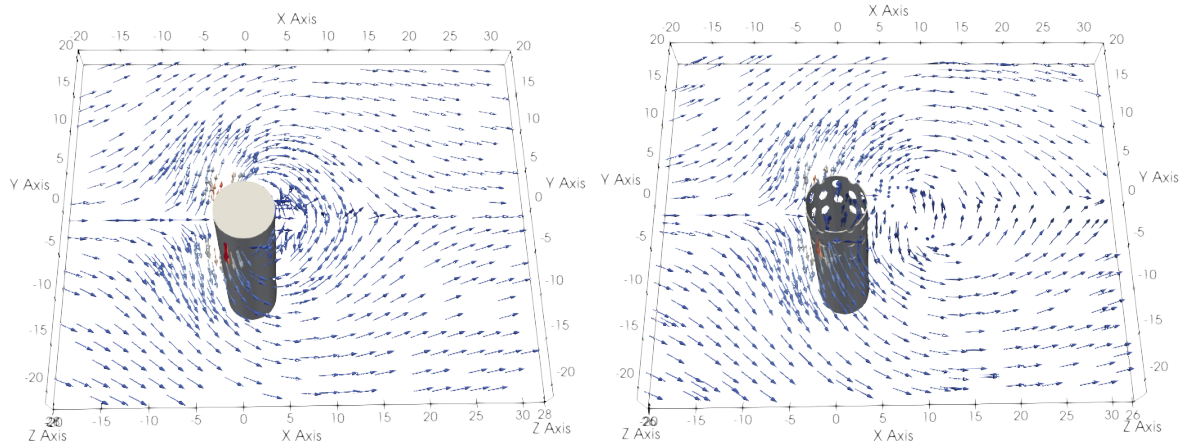

(a) Regular monopile (b) Perforated monopile

Figure 4.10: Vector field of the velocity, x-component is divided by 15 to be able to visualize the y- and z-components of the velocity, the figure does not show a scale as this has no meaning because of the recalculation of the velocity field. Red indicated high and blue indicates low yz-directed velocities

4.2.4. Wind Farm Scale

Figure 4.11 provides a perspective on how wake length relates to a real-world wind farm setting, specifically the Borssele III wind farm, where monopiles have diameters similar to the one assessed in this research. This figure indicates that the wakes are for the most part recovered into background conditions before reaching a neighboring monopile.

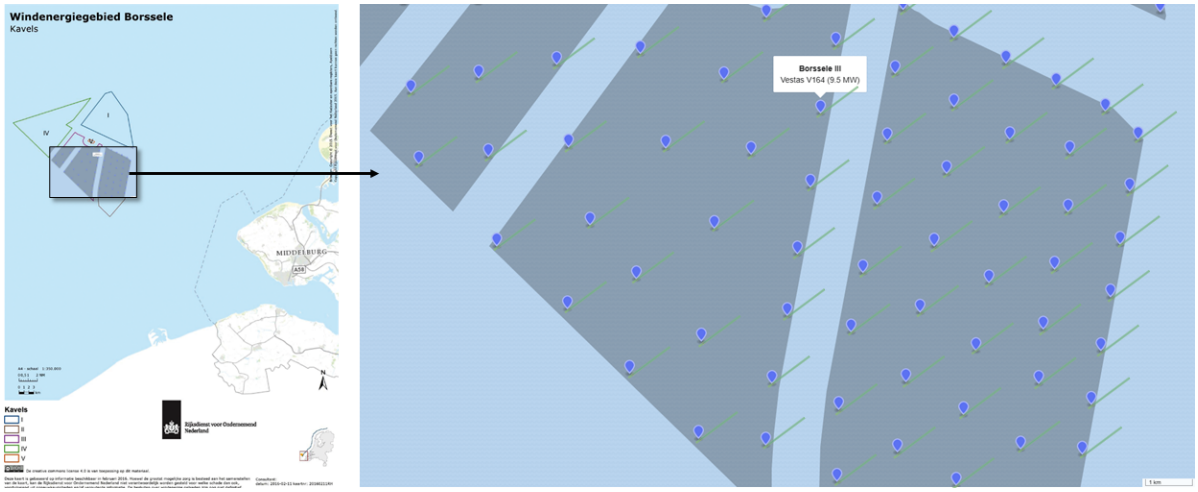

Figure 4.11: Wakes of 1000 m of the regular monopile design in the Borselle III wind farm, with monopiles diameters or around 7 to 8 m. Figure from [51], adapted by author.

4.3. Transverse Flow Profiles

As the transverse flow velocities are significantly smaller than the main flow velocity, U_x, it is important to analyze them separately.

4.3.1. Downflow

Downflow is one of these partially transverse flow properties. Downflow in front of a monopile is caused by the pressure differences induced by a logarithmic velocity profile, which arises from bed friction. Figure 4.12 presents the mechanism of the downflow through velocity vectors, where the x-directed velocity is divided by 1200 to be able to visualize the mechanism.

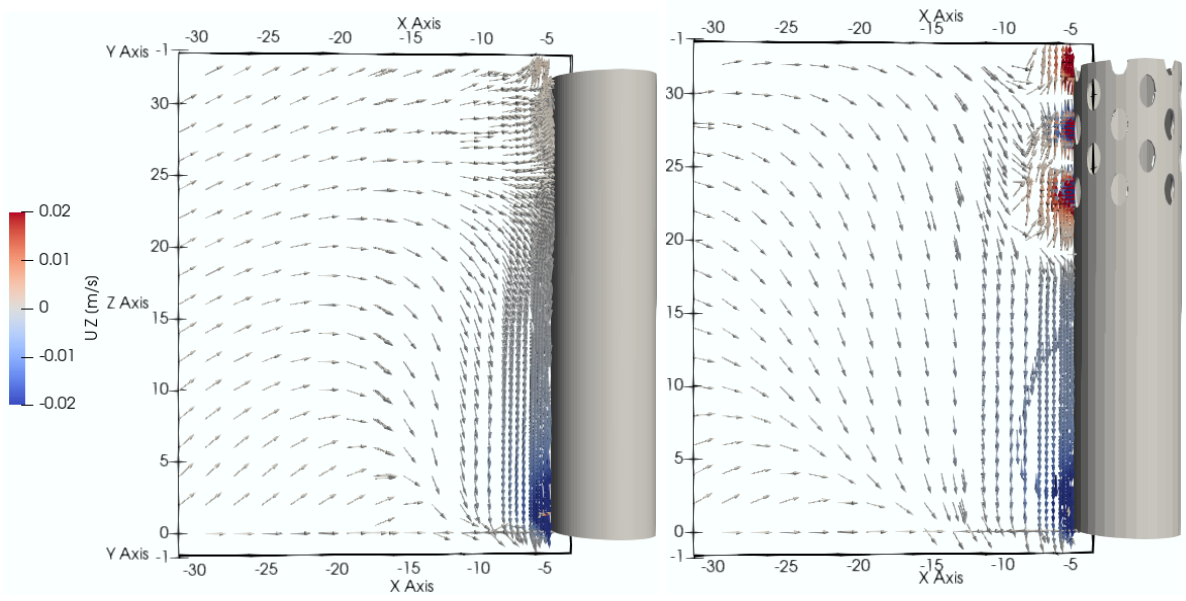

(a) Regular monopile (b) Perforated monopile

Figure 4.12: Vector visualization of the downflow in front of the monopiles. The horizontal component of the velocity is divided by 1200 to visualize the vertical components, the scale shows the z-directed velocity magnitude

Figure 4.13 is a visualization of the vertical velocity over depth for both regular and perforated monopile designs. The velocity data is taken 5 meters in front of the monopiles' vertical centerline, corresponding

to 1.5 meters in front of the monopile face (D = 7 m).

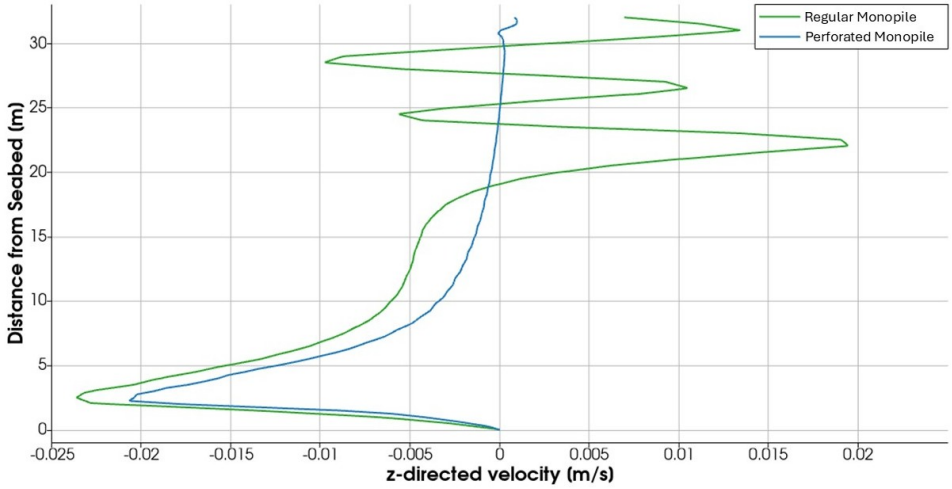

Figure 4.13: Upward directed flow velocity (downward is negative) over depth for the regular and perforated designs, 5 m in front of the monopile vertical centerline, meaning 1.5 m in front of the monopile (D = 7 m)

Below, the flow in front of the monopiles is broken down into three sections, focusing on the perforated design.

Section 32 m > z $\geq$ 19 m
In the top area, so between 19 m to 32 m, the flow velocity upstream of the holes increases, as depicted in Figure 4.14. This is caused by a form of the ”Venturi Effect”. The increased flow velocity upstream of the holes also accelerates streamlines located parallel to themselves. One can observe the upward and directed streamline parallel to those at the height of the perforations. At the same time, the acceleration upstream of the holes also leads to accelerated flow to deflect into a lower region. For all holes it holds that the z-directed flow velocity upstream of the perforated monopile is upward directed just below the holes and downward directed right above the holes.

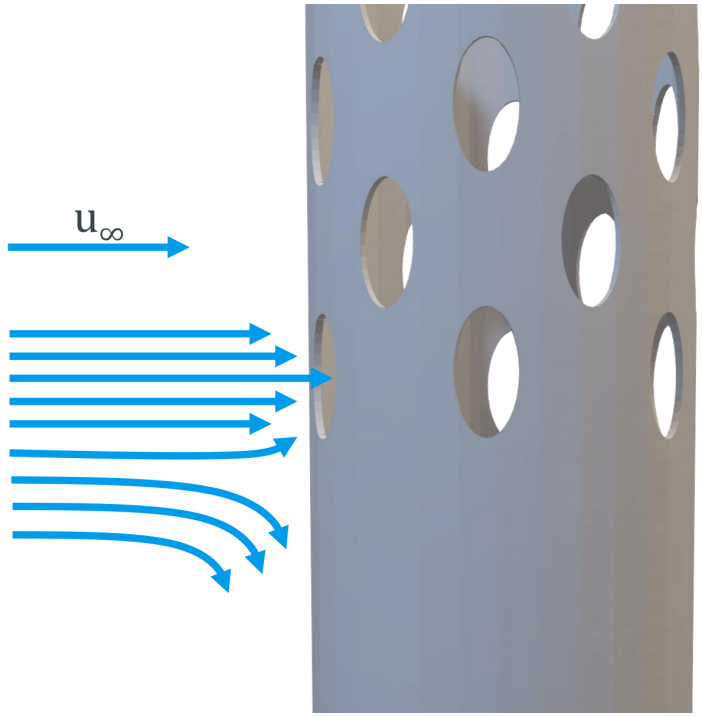

Figure 4.14: Streamlines of the flow upstream of one of the holes. Longer arrows mean higher velocities. This is not on scale. u_∞ = free-stream velocity.

Section 19 m > z $\geq$ 6 m
Below 19 m, the downflow for the perforated monopile is larger than for the regular monopile. This is caused by the contribution of the downward directed flow coming from the flow acceleration described above. From about 10 m and lower, the increase of the downflow magnitude follows a similar gradient as that for the regular monopile.

Section 6 m > z > 0 m
In the lowest section of the water column (z < 6 m), the downflow for the perforated monopile is also larger, $\frac{0.023}{0.0206} - 1 = 12\%$, to be specific. This could lead to an increased load on the bed protection and to increased scour hole formation.

For shallower waters, it is not expected that the perforations will lead to an increased downflow velocity, as in that case a larger portion of the perforations are located in a part of the water column in which the velocity profile is less developed, so more logarithmic. In this case, the perforations could reduce the downflow, compared to a regular monopile.

4.3.2. Downstream transverse profiles
Figure 4.15 illustrates the yz-directed flow velocity at 100 m downstream. Both wakes show clear horseshoe vortices, arising from the downflow. The maximum yz-velocity magnitude is slightly higher for the perforated design.

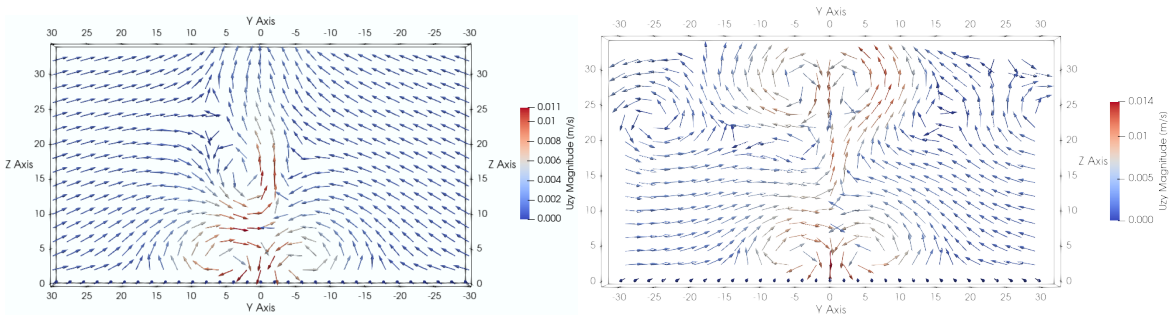

(a) Regular Monopile (b) Perforated Monopile

Figure 4.15: Vector visualization of y- and z-components of the flow, 100 m downstream of the monopiles, scales show the yz-directed velocity magnitude

4.4. Turbulence Parameters

This section displays the important parameters, which are the Turbulence Kinetic Energy (TKE or k), the Specific Turbulence Dissipation Rate (ω) and the Turbulent Eddy Viscosity (ν_t)

4.4.1. Turbulence Kinetic Energy (TKE)

The Turbulence Kinetic Energy (TKE) comparison, depicted in Figure 4.16, highlights the contrasting impact of both monopile designs. The regular monopile generates a relatively large amount of TKE behind the monopile, which persists until further downstream than the perforated design, which is in line with the velocity wake results. The TKE generated by the perforated design is highest within the monopile, caused by complex flow patterns inside. The peak behind the monopile (second peak) however, is relatively small compared to that of the regular monopile. This is why the TKE for the perforated design diminishes relatively fast and reaches background conditions.

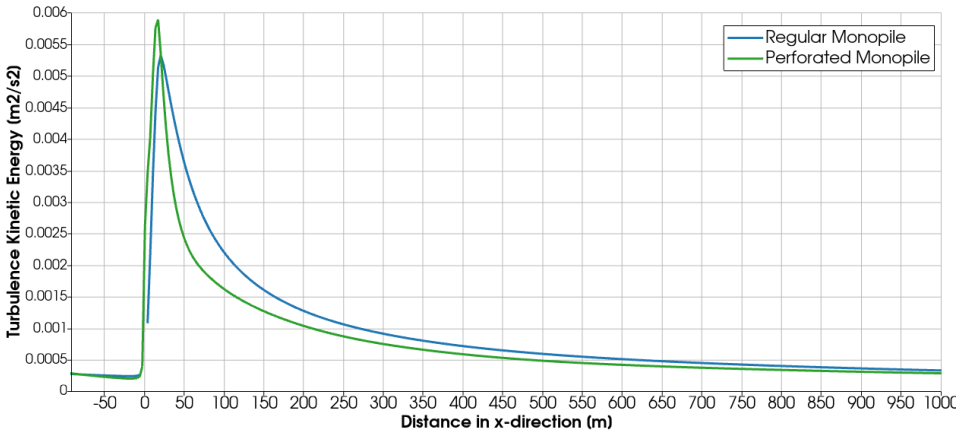

Figure 4.16: Turbulence Kinetic Energy of the Perforated and Regular monopile of the downstream (x) direction through the center of the monopile.

Figure 4.17 shows a top view the development of the TKE over the wake region of both the regular and perforated design. From these figures it can be seen how the TKE diminishes over the downstream direction. The perforated design creates a stronger wake just downstream of the monopile, but the TKE created by the regular design is higher from 55 m downstream and onward. This is most probably caused by smaller scale turbulence which is expected to be created by the perforations, which tends to dissipate faster. The larger eddies from the regular monopile travel further downstream before they dissipate through the energy cascade.

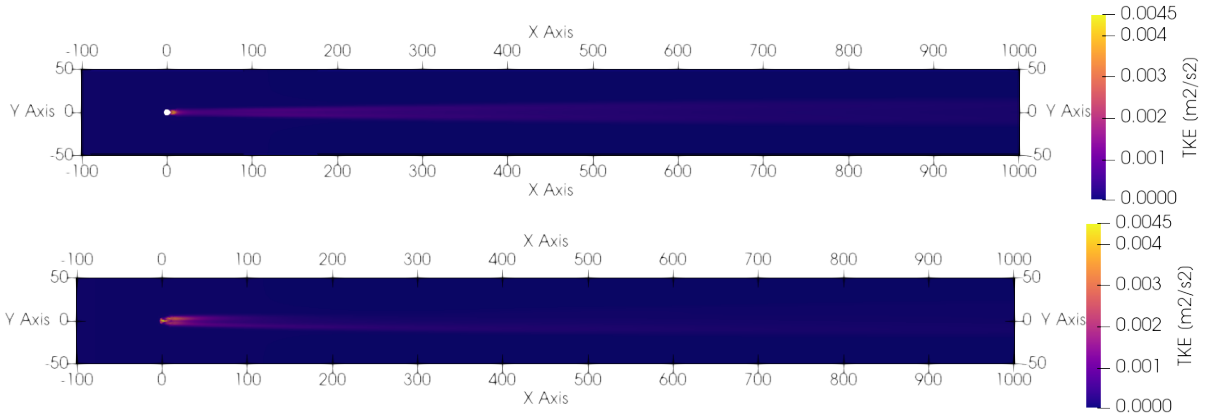

Figure 4.17: Turbulence Kinetic Energy in the wake of the Regular monopile (top) and the perforated monopil3 (bottom), z-slice (top view)

Figure 4.18 are close-ups of Figure 4.17 and highlight how the turbulence kinetic energy behaves just downstream of both monopile designs. As stated before in subsection 4.2.2, the jets coming through the perforations interact with the downstream flow. The result of this is visible in Figure 4.18b, where the TKE convects downstream in two separate paths, where flow stabilization is occurring in the middle.

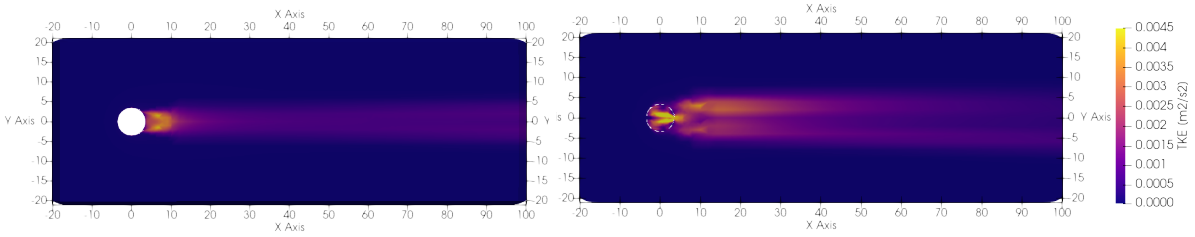

(a) Regular monopile (b) Perforated monopile

Figure 4.18: Close-up Turbulence Kinetic Energy wake of the regular and perforated monopiles, z-slice at a water depth of 2 m

Figure 4.19 are side views of the vertical distribution of the TKE. The regular monopile creates a turbulent field behind it over the entire depth. The perforated cylinder generates high TKE inside the perforations due to large shear between the jets and the slowly moving water in the monopile below and above the jets. The size of turbulent eddies generated by the perforations in the top part of the water column is expected to be in the order magnitude of the perforations, explaining why is dissipates quick relatively to the turbulence generated by the regular foundation.

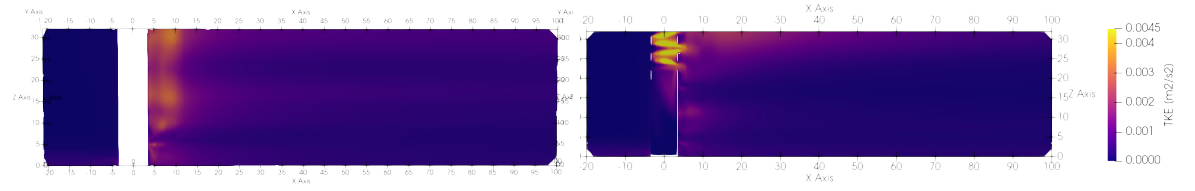

(a) Regular monopile (b) Perforated monopile

Figure 4.19: Side views (y-slices) of the Turbulence Kinetic Energy Wake of the regular and perforated monopiles

4.4.2. Specific Dissipation Rate

Figure 4.20 displays the specific turbulence dissipation rate ω for both designs. The turbulence in the wake of the perforated dissipates quicker, which is expected as the perforations are expected to create smaller scale turbulence which decays faster. The graphs meet each other at about 400 m downstream,

indicating that by then the small scale turbulence is mostly dissipated and mainly the larger eddies from the vortex shedding are still present in the wake.

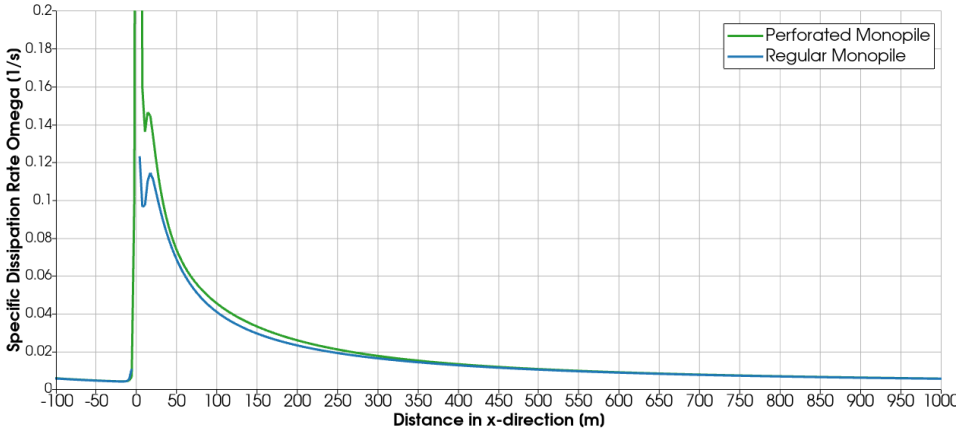

Figure 4.20: Specific Dissipation Rate ω of the Perforated and Regular monopile of the downstream (x) direction through the center of the monopile at an elevation of z = 25 m. The peak of $\omega_{perforated}$ extends until 0.9 [1/s]

4.4.3. Turbulent Eddy Viscosity

The decay of the turbulent eddy viscosity ν_t is shown in Figure 4.21. The perforated design shows a drop in ν_t in the near wake region (0 > x > 200 m), which is due to the high dissipation rates in this region. After this initial drop the eddy viscosity gets back to the slower decay of large scale turbulence, which explains why it increases again even though the TKE decreases.

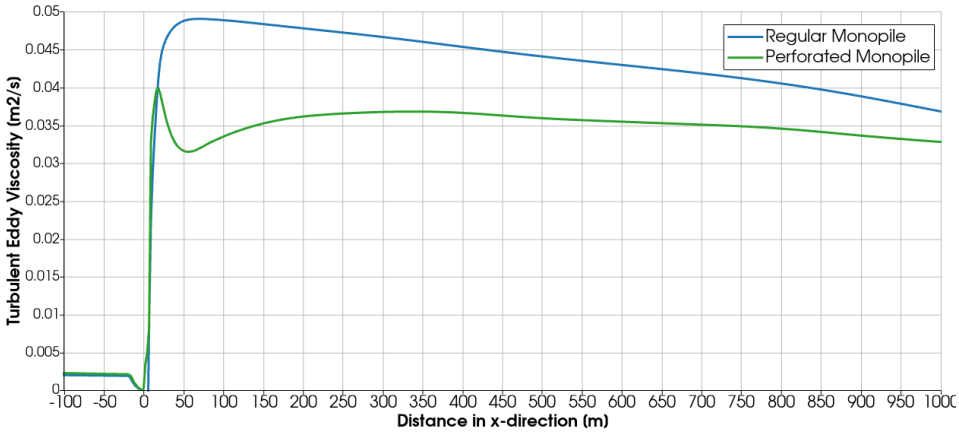

Figure 4.21: Turbulent Eddy Viscosity ν_t of the Perforated and Regular monopile of the downstream (x) direction through the center of the monopile

4.4.4. Combined

Figure 4.22 displays the three turbulence parameters until 3000 m downstream for the regular monopile and no thermal stratification. The figure shows how they relate. It is expected that the model slightly underestimates the turbulence dissipation ω, which could explain why ν_t stays elevated until far downstream.

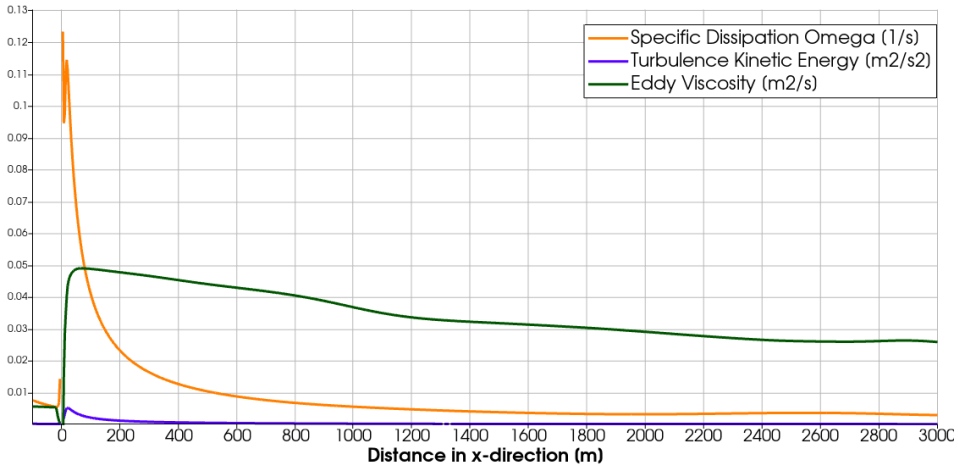

Figure 4.22: ν_t, TKE and ω for the regular monopile combined in one figure, until 3000 m downstream

4.5. Thermal Stratification

This section presents the impact of a regular monopile and a perforated monopile on the thermal changes of the water column. The results are analyzed using the Relative Destratification (RD) metrics, as outlined in subsection 3.4.4.

4.5.1. Regular monopile

Figure 4.23 shows a top view of the computational domain with the regular monopile for the case with a temperature gradient of ΔT = 0.5 K. It displays how the temperature mixing develops in downstream direction. The simulations for the stronger thermocline behave in a similar way, hence only one top view is shown.

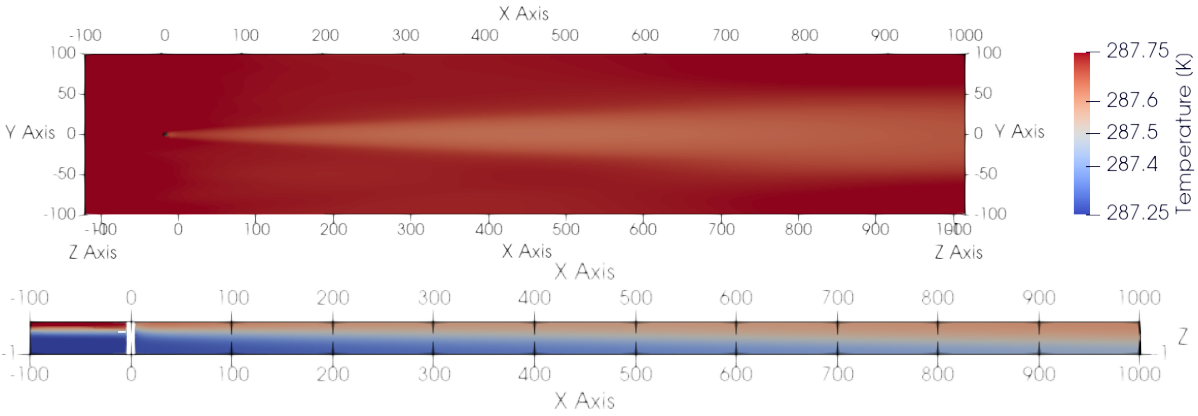

Figure 4.23: Top view and side view of the temperature in the computational domain for the regular monopile

Table 4.3 presents the Relative Destratification (RD) values for different initial stratification conditions. An RD value of 38.59% occurs for ΔT = 0.5 K, showing that close to half of the original temperature gradient is lost in the wake region. However, as the initial stratification strength increases, the RD value decreases, with RD = 27.37% for ΔT = 3.5 K.

Table 4.3: Simulation results of the regular monopile, showing the Relative Destratification, see subsection 3.4.4. The values are in Kelvin, except when stated differently

Case & Scenario	T(-50,0,32)	T(500,0,32)	T_{RD}	RD [%]
Regular, ΔT=0.5	287.75	287.56	0.19	38.59
Regular, ΔT=1.5	287.75	287.24	0.51	34.04
Regular, ΔT=2.5	287.75	286.98	0.77	30.90
Regular, ΔT=3.5	287.75	286.79	0.96	27.37

4.5.2. Perforated Monopile

Figure 4.24 shows a top view of the computational domain with the perforated monopile for the case with a temperature gradient of ΔT = 0.5 K. The temperature wake is slightly less pronounces when compared to the regular monopile.

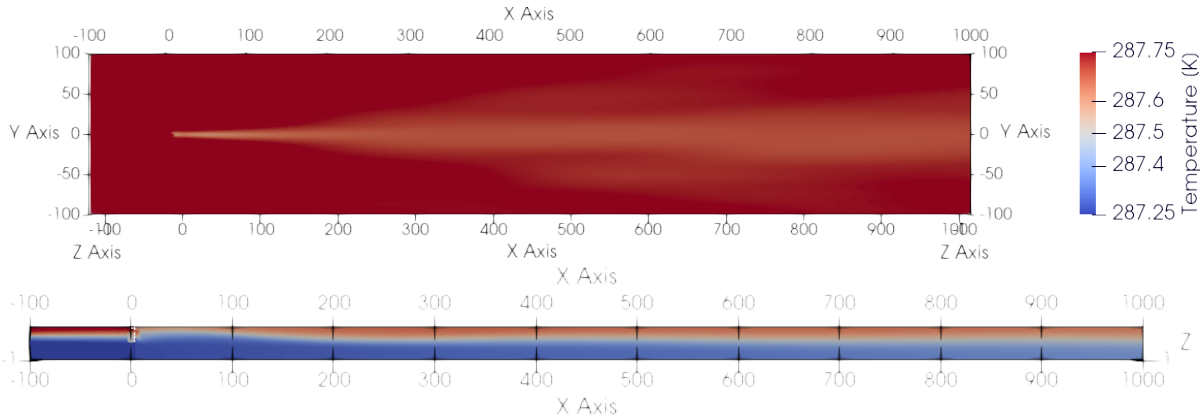

Figure 4.24: Top view and side view of the temperature in the computational domain for the perforated monopile

Table 4.4 shows the RD values for the perforated monopile case. At ΔT = 0.5 K, the perforated monopile exhibits a RD of 29.18% and at ΔT = 3.5 K, the RD has a value of 24.81%, meaning that the RD decreases for increasing temperature.

Table 4.4: Simulation results of the perforated monopile, showing the Relative Destratification, see subsection 3.4.4. The values are in Kelvin, except when stated differently

Case & Scenario	T(-50,0,32)	T(500,0,32)	T_{RD}	RD [%]
Regular, ΔT=0.5	287.75	287.60	0.15	29.18
Regular, ΔT=1.5	287.75	287.34	0.41	27.32
Regular, ΔT=2.5	287.75	287.11	0.64	25.64
Regular, ΔT=3.5	287.75	286.88	0.87	24.81

4.5.3. Comparison

The amount of destratification is more for all scenarios for the regular monopile. The difference is on average approximately 0.1 K for all scenarios, as seen in Figure 4.25.

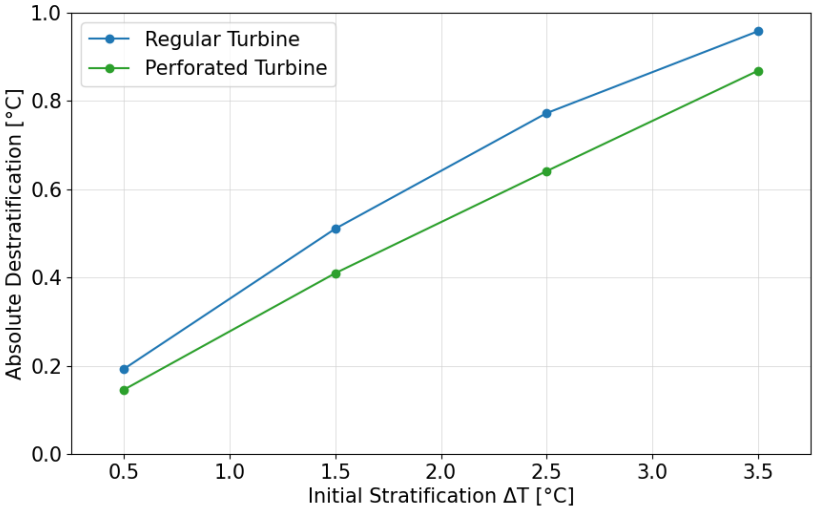

Figure 4.25: Absolute destratification for the regular and perforated designs for different stratification strengths

The difference is most pronounced in weak stratification conditions, where the perforated monopile achieves a reduction in RD by up to 9.41% compared to the regular one. However, as ΔT increases, the difference between the two designs decreases. These findings suggest that perforated monopiles could be effective in reducing destratification in environments where stratification is weak to moderate.

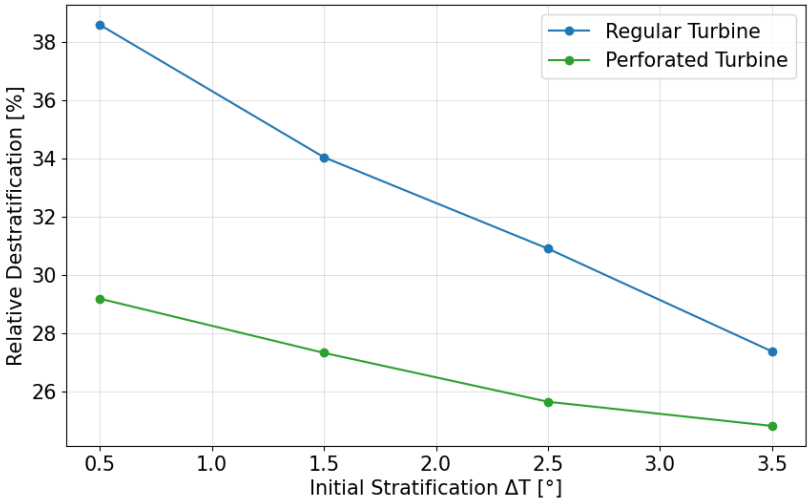

Figure 4.26: Relative Destratification for the regular and perforated designs for different stratification strengths

5
Discussion

This discussion section interprets the key findings of this study, examining their implications for offshore wind farm hydrodynamics and marine ecosystem interactions. The results highlight the differences in wake recovery, turbulence generation, vertical velocity structures, and thermal destratification between regular and perforated monopile designs. Furthermore, this section addresses the ecological and engineering implications of these findings and critically assesses the study's assumptions and limitations.

5.1. Interpretation of Key Findings

This section discusses the main findings of this study. The results provide insights into the hydrodynamic wake behavior of monopiles, their influence on thermal stratification and the role of initial stratification conditions in determining the extent of destratification.

5.1.1. Wake and Flow Recovery

One of the key findings of this study is the significant difference in velocity wake characteristics between regular monopiles and perforated monopiles.

- The regular monopile generates a stronger and longer wake, with increased turbulence and delayed velocity recovery downstream. The wake is recovered to 90% of the free-stream velocity after 660 meters downstream.
- The perforated monopile design reduces wake intensity and leads to a shorter wake length, implying faster recovery of the free-stream velocity. It is recovered to 90 % of the free-stream velocity at 210 meters downstream.

This relatively fast recovery can be attributed to the perforations. The water flowing through interacts with the recirculation zone, reducing negative x-velocities, as seen from Figure 4.10. This leads to less flow recirculation and in turn less flow separation. This reduced flow separation leads in turn to lower generation of turbulence. Besides that, Figure 4.9 show that the perforations lead to a reduction of the flow velocity around the monopile in the top part, which can also lead to generation of less turbulence. Furthermore, the perforations generate smaller scale turbulence and less monopile diameter scale turbulence relative to the regular monopile, which decays faster into heat. This is substantiated by Figure 4.20 and Figure 4.21. The former indicating high TKE dissipation in the near-wake and the latter showing how the eddy viscosity dips in the near-wake.

5.1.2. Transverse Flow Profiles

Analyzing the transverse profiles, there are slight differences noticeable between the regular and perforated monopile. Both in terms of downflow and in downstream transverse profiles. as seen from Figure 4.12 and Figure 4.15 however, the differences are small when put into perspective with the x-directed flow velocity. Therefore these processes are not expected to influence the thermal stratification significantly.

5.1.3. Effect of Initial Stratification

The strength of initial stratification plays a role in determining the extent of destratification induced by monopile turbulence. The results found in Figure 4.26 indicate that cases with higher initial stratification experience lower Relative Destratification (RD). The density differences create buoyancy forces that resist vertical motion, as stated in subsection 1.1.3. As a result, even though turbulence is gener-

ated by the monopiles, its ability to induce mixing is constrained by buoyancy forces, leading to lower RD values in strongly stratified cases. These findings underscore the importance of considering background stratification when assessing the impact of offshore wind farms on vertical mixing, as especially in weakly stratified waters, the influence of wind turbine foundations can be large. However, it is unsure if mixing already weakly stratified waters has serious impact.

5.1.4. Effect of Monopile Design on Destratification

As seen from section 4.5, the perforated monopile has a mitigating effect on the destratification when compared to the regular monopile. The reduction in destratification is approximately 0.1 K on average for all four scenarios.

From the Relative Destratification it follows that this mitigating effect is relatively larger for weakly stratified waters. In the weakly stratified scenarios the reduced turbulent eddy viscosity in the wake of the perforated monopile has a relatively higher mitigating impact when compared to the scenarios with stronger initial stratification.

Weaker initial stratification leads to a higher Relative Destratification (RD) as stated above, however, this effect is more pronounced for the regular monopile than for the perforated one.

This highlights an important consideration for offshore wind farm designs in stratified environments. In areas with naturally weak stratification, regular monopiles may contribute more aggressively to destratification. In these environments, perforated monopile designs could play a role. On the contrary, in regions with strong stratification, the differences between monopile designs may be less relevant. This shows that the influence of structural modifications must be put in context with the initial stratification conditions.

5.2. Ecological Implications

Adding perforations to monopiles could have both negative and positive effects on ecology. The ecological implications found in this research and literature are stated below.

Positive Effects

- The reduced turbulence from the perforated design could lead to a reduced increase in suspended sediment content in the water column, however, this has to be assessed.
- The perforations could act as a habitat for marine life.
- Monopile perforations are able to mitigate destratification in weakly stratified waters, possibly enhancing phytoplankton growth when compared to regular monopile designs.
- The reduced mixing due to the perforations could help in sustaining the colder underlayer, which is home to species.

Negative Effects

- Perforations increase downflow in front of the monopile, which could stir up more sediments leading to less light intrusion in the water column, which could lead to a lower production of phytoplankton.
- Several sources state that the increased mixing could have a positive effect on phytoplankton growth and with that on the entire food chain as water column stability could limit nutrient availability and oxygen levers in the lower part of the water column. Mixing mitigation by perforated monopiles could therefore have negative impacts. [14] [18]

A rather neutral effect is that adding perforations to the foundations is found to not have significant effects on stratification in strongly stratified waters

All the effects are uncertain and require thorough, site-specific, ecological investigations towards for example limiting factors on phytoplankton growth. In some regions the limiting factor could be nutrient availability, whereas in other regions it could be light intrusion.

5.3. Engineering Implications

From an engineering perspective, adding perforations to a monopile adds many complications but can also be an opportunity. The positive and negative effects of adding holes outlined again below:

Negative Effects

- Requires extra attention during installation because of increased stresses around the holes.
- Requires a more intensive manufacturing process.
- Biofouling in the interior surfaces of the perforated design could increase hydrodynamic drag, leading to increased loading.
- Could lead to complications with respect to the cable, as it is now subject to hydrodynamic forces.

Positive Effects

- Perforations can reduce wave loading.
- The replenishment of water through the holes can reduce the risk of differential aeration corrosion and can increase the effectiveness of cathodic protection systems, also controlling corrosion.

5.4. Assumptions and Limitations

In interpreting the results of this study, several assumptions were made regarding the physical and numerical aspects of the models. These assumptions influence the accuracy and applicability of the findings and should be considered when extrapolating the results to real-world scenarios.

- Tidal and Wind-Driven Currents.
  - A constant tidal current is assumed, whereas in reality, tides are dynamic on both daily ad monthly time scales. These variations could alter the velocity field and destratification behavior.
- Salinity Effects
  - The models assume a constant salinity, whereas in reality, salinity gradients contribute to buoyancy forces and can modify the mixing and stratification dynamics.
- Turbulence Model Limitations.
  - The study employs turbulence models (RANS-based), which introduce inaccuracies due to their assumptions of eddy viscosity. Large eddy simulations (LES) or direct numerical simulations (DNS) would provide higher accuracy but at a much greater computational cost.
- Model Setup Limitations.
  - Due to the size of the researched domain, concessions were made on the grid resolution to make the computations feasible. This could cause outcomes which are not completely realistic.
- Stratification Evolution Over Time.
  - The study focuses on a specific stratification state, but in natural systems, stratification develops and weakens seasonally. Future studies should assess stratification over a full season, considering its natural evolution.
- Influence of Marine Growth.
  - The study does not consider the effect of marine growth (e.g., biofouling) on monopiles. Accumulation of marine organisms could alter flow dynamics within and around perforations, influencing wake turbulence and mixing. This could potentially have a greater effect on the perforated design than on the regular monopiles
- Suspended Sediment and Light Penetration.

– The study does not explicitly assess the impact of increased downflow and reduced turbulence on suspended sediment transport. A lower turbulence intensity could lead to less sediment resuspension, whereas increased downflow could enhance the resuspension of sediments. This could have an influence on light penetration in the water column, which could have ecological consequences.

6
Conclusion

This conclusion section synthesizes the key insights from the study, summarizing the main findings and their implications for offshore wind turbine foundation design and environmental sustainability. By addressing the research objectives and questions, the conclusion provides a concise summary of the study's contributions while outlining potential directions for future research and practical applications.

How do perforated monopile designs influence seawater stratification when compared to regular monopiles?

6.1. Conclusion

To address the main research question, it is essential to first answer the supporting research questions.

The first supporting research question, "What hydrodynamic mechanisms contribute to the destratification of seawater caused by monopiles, and how does a perforated design influence these mechanisms?", was addressed through wake analysis. It was found that the turbulence parameter turbulent eddy viscosity is the main proxy for vertical mixing. For the regular monopile this parameter is influenced by the turbulence generated when the water flows around the monopile. For the perforated monopile however, the results of this research indicate that the perforations have a mitigating effect on the wake through several mechanisms. These mechanisms include reduced recirculation, reduced flow around the monopile leading to lower turbulence and the generation of smaller scale turbulence due to the perforations, decaying faster.

The second supporting question, "How does initial stratification strength influence destratification rates for regular and perforated monopiles?", is answered through examining the impact of initial stratification on monopile-induced mixing. The results confirm that stronger initial stratification reduces relative destratification. This is attributed to buoyancy forces counteracting vertical mixing, limiting the impact of both turbulent mixing. It was also found that the perforated monopile has a more mitigating effect for weakly stratified scenarios.

When integrating these findings, it becomes clear that while perforated monopile designs do offer some benefits in mitigating the impact on seawater stratification, the effects are relatively small. The reduced turbulence due to perforations contribute to less vertical mixing. However, the overall impact is not substantial enough to definitively recommend a significant design change. Nevertheless, the minor benefits observed could still be advantageous in specific scenarios where even small reductions in environmental disruption are valuable. Future research should continue to explore these designs to optimize their effectiveness and assess their long-term ecological impacts, while also considering the cost-benefit ratio of implementing such modifications in offshore wind energy projects.

6.2. Broader Context and Impact

The findings of this research contribute to a deeper understanding of the interactions between offshore wind turbine foundations and ocean stratification. As the offshore wind industry expands, the role of monopile-induced mixing in marine ecosystems becomes increasingly relevant. This study provides insight into how different monopile designs influence destratification and, by extension, the surrounding marine environment.

From an ecological perspective, the study highlights that offshore wind turbine foundations alter thermal

stratification, which can impact nutrient cycling, oxygen distribution, and marine biodiversity. However, the limited effectiveness of perforated monopiles in mitigating destratification suggests that their deployment would not be a feasible method for mitigating stratification-related ecological concerns. This is particularly the case for regions where a stronger thermocline develops.

From an engineering standpoint, this research underscores the trade-offs involved in designing monopile structures. Structural complexities, installation challenges, and potential biofouling issues must be carefully weighed against the potential ecological benefits.

Overall, this research underscores that while offshore wind turbines contribute to global sustainability efforts, their localized environmental impacts require careful consideration. The limited destratification mitigating potential of perforated monopiles suggests that alternative engineering solutions may be necessary to minimize ecological consequences.

6.3. Recommendations for Future Research

While this study provides valuable insights into the influence of monopile designs on stratification and wake turbulence, several areas require further investigation to refine these findings and expand their applicability.

- **Field Validation and Experimental Studies**
  - Conducting more field validation to compare model predictions with real-world measurements from offshore wind farms.
  - Performing laboratory-scale research, particularly if field validation is not feasible, to analyze turbulence and mixing for a perforated monopile under controlled conditions.
- **Enhanced Numerical Modeling for Increased Accuracy**
  - Implementing Large Eddy Simulations (LES) to better capture turbulent structures.
  - Investigating the effects of different velocity conditions to assess model sensitivity to inflow conditions.
- **Expanded Environmental Considerations**
  - Evaluating the impact of tidal cycles, rather than assuming a steady current, to better reflect real-world hydrodynamic conditions.
  - Including salinity effects in buoyancy calculations to better represent oceanic stratification.
  - Incorporating wave forcing, which plays a significant role in offshore mixing.
  - Accounting for wind-driven mixing, particularly in shallow waters where surface forcing can dominate. This means that the simulations should become multiphase.
  - Sediment resuspension should be investigated as extension of this research, as it can have strong influence on ecology.
  - Include marine growth on the different monopile designs into the research, as this could have a relatively larger effect on the perforated design.
  - Determining whether perforated designs are more effective in shallow waters, where velocity profiles develop differently due to the lower water depth. In this research expansion, besides the stratification, the downflow and its effect on the scour should be assessed.
  - Investigating how wake interactions evolve in full wind farm arrays, where monopile-induced turbulence may interact with multiple structures.
- **Ecological Considerations**
  - Investigating the ecological impact of different monopile designs, particularly in weakly stratified regions where perforated monopiles have a stronger effect.

  - Evaluating whether the difference in destratification at low stratification levels (e.g. 0.5 K) is ecologically significant, as the importance of such small temperature variations remains unclear.

- **Engineering Design Considerations**
  - Different monopile sizes should be investigated to assess the sensitivity of the outcomes on the foundation diameter.
  - Include several perforation sizes and amounts to assess the sensitivity of the outcomes on this parameters.

By addressing these areas, future research can provide a more complete understanding of monopile-induced hydrodynamic changes, allowing for improved design optimizations and ecological impact assessments in offshore wind farms.

Bibliography

[1] AirShaper Flow Separation Boundary Layer Seperation, https://airshaper.com/. URL: https://airshaper.com/.

[2] Leye M. Amoo and R. Layi Fagbenle. “12 - Advanced fluids – a review of nanofluid transport and its applications”. In: *Applications of Heat, Mass and Fluid Boundary Layers*. Ed. by R.O. Fagbenle et al. Woodhead Publishing Series in Energy. Woodhead Publishing, 2020, pp. 281–382. ISBN: 978-0-12-817949-9. DOI: https://doi.org/10.1016/B978-0-12-817949-9.00020-7. URL: https://www.sciencedirect.com/science/article/pii/B9780128179499000207.

[3] “An Internet Book on Fluid Dynamics Potential Flow around a Cylinder”. In: ().

[4] Jacob Andersen et al. “Wave Load Mitigation by Perforation of Monopiles”. In: *Journal of Marine Science and Engineering 2020, Vol. 8, Page 352* 8.5 (May 2020), p. 352. ISSN: 2077-1312. DOI: 10.3390/JMSE8050352. URL: https://www.mdpi.com/2077-1312/8/5/352/htm%20https://www.mdpi.com/2077-1312/8/5/352.

[5] J.D. Anderson. *Computational Fluid Dynamics: The Basics with Applications*. McGraw-Hill International Editions: Mechanical Engineering. McGraw-Hill, 1995. ISBN: 9780071132107. URL: https://books.google.fr/books?id=phG_QgAACAAJ.

[6] *FLUIDS, Basics of Turbulent Flows*. ANSYS LECTURES, FLUIDS, Basics of Turbulent Flows.

[7] Jaywant Arakeri and P. Shankar. “Ludwig Prandtl and boundary layers in fluid flow”. In: *Resonance* 5 (May 2012), pp. 48–63. DOI: 10.1007/BF02840395.

[8] Martin J Austin et al. “Enhanced bed shear stress and mixing in the near wake of an offshore wind turbine monopile”. In: (2024). DOI: 10.5194/egusphere-2024-2056. URL: https://doi.org/10.5194/egusphere-2024-2056.

[9] L. Balas and E. Özhan. “Three-dimensional modelling of stratified coastal waters”. In: *Estuarine, Coastal and Shelf Science* 54.1 (2001), pp. 75–87. ISSN: 02727714. DOI: 10.1006/ecss.2001.0832.

[10] Jiri Blazek. “Chapter 7 - Turbulence Modeling”. In: *Computational Fluid Dynamics: Principles and Applications (Third Edition)*. Ed. by Jiri Blazek. Third Edition. Oxford: Butterworth-Heinemann, 2015, pp. 213–252. ISBN: 978-0-08-099995-1. DOI: https://doi.org/10.1016/B978-0-08-099995-1.00007-5. URL: https://www.sciencedirect.com/science/article/pii/B9780080999951000075.

[11] Ruddy Brionnaud. “Introduction to the Lattice-Boltzmann Method and technology overview of the CFD software XFlow”. In: (2015).

[12] Wei Chen et al. “The role of heat wave events in the occurrence and persistence of thermal stratification in the southern North Sea”. In: *Natural Hazards and Earth System Sciences* 22.5 (May 2022), pp. 1683–1698. ISSN: 16849981. DOI: 10.5194/NHESS-22-1683-2022.

[13] T.J. Craft, B.E. Launder, and K. Suga. “Development and application of a cubic eddy-viscosity model of turbulence”. In: *International Journal of Heat and Fluid Flow* 17.2 (1996), pp. 108–115. ISSN: 0142-727X. DOI: https://doi.org/10.1016/0142-727X(95)00079-6. URL: https://www.sciencedirect.com/science/article/pii/0142727X95000796.

[14] Ute Daewel et al. “Offshore wind farms are projected to impact primary production and bottom water deoxygenation in the North Sea”. In: *Communications Earth & Environment 2022 3:1* 3.1 (Nov. 2022), pp. 1–8. ISSN: 2662-4435. DOI: 10.1038/s43247-022-00625-0. URL: https://www.nature.com/articles/s43247-022-00625-0.

[15] Pauline M. Doran. “Chapter 7 - Fluid Flow”. In: *Bioprocess Engineering Principles (Second Edition)*. Ed. by Pauline M. Doran. Second Edition. London: Academic Press, 2013, pp. 201–254. ISBN: 978-0-12-220851-5. DOI: https://doi.org/10.1016/B978-0-12-220851-5.00007-1. URL: https://www.sciencedirect.com/science/article/pii/B9780122208515000071.

[16] T Ebdon et al. “Wake measurement metrics and the dependence of tidal turbine wakes on turbine operating condition”. In: ().

[17] The Editors of Encyclopaedia Britannica. “Thermocline”. In: *Britannica* (2013).

[18] David Fields et al. “Authors and Affiliations: Oceanographic Effects of Offshore Wind Structures and Their Potential Impacts on the North Atlantic Right Whale and Their Prey”. In: ().

[19] URL: https://discretize.simpeg.xyz/en/main/content/finite_volume.html.

[20] URL: https://www.youtube.com/watch?v=QhI7OybaI1s.

[21] Leap Australia, What y+ should I use? Part 1 – Understanding the physics of boundary layers, https://www.leapaust.com.au/blog/cfd/y-plus$_{p}art1_{u}nderstanding-the-physics-of-boundary-layers/$.

[22] SimScale, K-Omega-SST Turbulence Models, https://www.simscale.com/docs/simulation-setup/global-settings/k-omega-sst/.

[23] IRENA. *Global energy transformation : a roadmap to 2050*. International Renewable Energy Agency, 2019, p. 51. ISBN: 9789292601218.

[24] Shamoon Jamshed. “Chapter 4 - High Reynolds Number Flows”. In: *Using HPC for Computational Fluid Dynamics*. Ed. by Shamoon Jamshed. Oxford: Academic Press, 2015, pp. 81–100. ISBN: 978-0-12-801567-4. DOI: https://doi.org/10.1016/B978-0-12-801567-4.00004-0. URL: https://www.sciencedirect.com/science/article/pii/B9780128015674000040.

[25] Yuyao Jiang, James Percival, and Stephan Kramer. *A comparison of RANS and URANS turbulence models for flow past a circular cylinder in OpenFOAM*. Tech. rep. 2023.

[26] Sachin Jindal et al. “Geotechnical challenges in monopile foundations and performance assessment of current design methodologies”. In: *Ocean Engineering* 310 (Oct. 2024), p. 118469. ISSN: 0029-8018. DOI: 10.1016/J.OCEANENG.2024.118469.

[27] Nikolaos D. Katopodes. “Chapter 8 - Turbulent Flow”. In: *Free-Surface Flow*. Ed. by Nikolaos D. Katopodes. Butterworth-Heinemann, 2019, pp. 566–650. ISBN: 978-0-12-815489-2. DOI: https://doi.org/10.1016/B978-0-12-815489-2.00008-3. URL: https://www.sciencedirect.com/science/article/pii/B9780128154892000083.

[28] John T. O. Kirk. “Light and Photosynthesis in Aquatic Ecosystems”. In: (1994). DOI: 10.1017/CBO9780511623370. URL: https://www.cambridge.org/core/books/light-and-photosynthesis-in-aquatic-ecosystems/C19B28AE07B1CDEBDA5593194DE4E304.

[29] Marcello Lappa. “Incompressible flows and the Boussinesq approximation: 50 years of CFD”. In: *Comptes Rendus - Mecanique* 350.S1 (2022), pp. 1–22. ISSN: 18737234. DOI: 10.5802/CRMECA.134/. URL: https://doi.org/10.5802/crmeca.134http://creativecommons.org/licenses/by/4.0/LesComptesRendus.M%C3%A9caniquesontmembresduCentreMersennepo
C3%A9ditionscientifiqueouvertewww.centre-mersenne.org.

[30] Guancheng Li et al. *Increasing Ocean Stratification Over the Past Half Century*. Tech. rep. 2020.

[31] Bingchen Liang et al. “Local Scour for Vertical Piles in Steady Currents: Review of Mechanisms, Influencing Factors and Empirical Equations”. In: *Journal of Marine Science and Engineering 2020, Vol. 8, Page 4* 8.1 (Dec. 2019), p. 4. ISSN: 2077-1312. DOI: 10.3390/JMSE8010004. URL: https://www.mdpi.com/2077-1312/8/1/4/htm%20https://www.mdpi.com/2077-1312/8/1/4.

[32] Travis Miles et al. “Offshore wind energy and the mid-atlantic cold pool: A review of potential interactions”. In: *Marine Technology Society Journal* 55.4 (July 2021), pp. 72–87. ISSN: 19481209. DOI: 10.4031/MTSJ.55.4.8.

[33] *Monopile, Jacket or Floater, how do I pick the right option for my offshore wind project? - Empire engineering*. URL: https://www.empireengineering.co.uk/monopile-jacket-or-floater-how-do-i-pick-the-right-option-for-my-offshore-wind-project/.

[34] URL: http://encyclopediaofmath.org/index.php?title=Ostrogradski_formula&oldid=31300.

[35] Alexander Paluzzi et al. "Effects of Perforations on Internal Cathodic Protection and Recruitment of Marine Organisms to Steel Pipes". In: *Journal of Marine Science and Engineering* 12.8 (Aug. 2024). ISSN: 20771312. DOI: 10.3390/jmse12081299.

[36] Joaquim Peiro and Spencer Sherwin. "Handbook of Materials Modeling, 8.2 Finite Difference, Finite Element and Finite Volume Methods for Partial Differential Equations". In: Jan. 2005, pp. 2415–2446. DOI: 10.1007/978-1-4020-3286-8_127.

[37] *Perforated Offshore Monopile for Corrosion Control, Marine Habitats*. URL: https://www.materialsperformance.com/articles/cathodic-protection/2019/04/perforated-offshore-monopile-for-corrosion-control-marine-habitats?utm_source=chatgpt.com.

[38] *Perforation of Monopiles to Reduce Hydrodynamic Loads and Enable use in Deep Waters | TU Delft Repository*. URL: https://repository.tudelft.nl/record/uuid%3A91eada6f-4f2b-4ae6-be59-2b5ff0590c6f?utm_source=chatgpt.com.

[39] C. Rogan et al. "The turbulent wake of a monopile foundation". In: *Renewable Energy* 93 (Aug. 2016), pp. 180–187. ISSN: 18790682. DOI: 10.1016/j.renene.2016.02.050.

[40] François G Schmitt. "About Boussinesq's turbulent viscosity hypothesis: historical remarks and a direct evaluation of its validity". In: *Comptes Rendus Mécanique* 335.9-10 (Oct. 2007), pp. 617–627. DOI: 10.1016/j.crme.2007.08.004. URL: https://hal.science/hal-00264386.

[41] L. K.P. Schultze et al. "Increased Mixing and Turbulence in the Wake of Offshore Wind Farm Foundations". In: *Journal of Geophysical Research: Oceans* 125.8 (Aug. 2020). ISSN: 21699291. DOI: 10.1029/2019JC015858.

[42] Jonathan Sharples et al. "Inter-annual variability in the timing of stratification and the spring bloom in the North-western North Sea". In: *Continental Shelf Research* 26.6 (Apr. 2006), pp. 733–751. ISSN: 02784343. DOI: 10.1016/j.csr.2006.01.011.

[43] Martin Skote and Stefan Heinz. "The Law of the Wall and von Kármán Constant: An Ongoing Controversial Debate". In: *Fluids 2024, Vol. 9, Page 63* 9.3 (Mar. 2024), p. 63. ISSN: 2311-5521. DOI: 10.3390/FLUIDS9030063. URL: https://www.mdpi.com/2311-5521/9/3/63/htm%20https://www.mdpi.com/2311-5521/9/3/63.

[44] Titi Sui et al. "3D numerical modeling of wave–monopile–seabed interaction in the presence of a scour hole". In: *Ocean Engineering* 298 (Apr. 2024). ISSN: 00298018. DOI: 10.1016/j.oceaneng.2024.117254.

[45] H.U. Sverdrup. "On Conditions for the Vernal Blooming of Phytoplankton". In: *Norsk Polarinstitutt* (1953).

[46] Skybrary. *Temperate oceanic climate (Cfb)*. URL: https://skybrary.aero/articles/temperate-oceanic-climate-cfb-0.

[47] "The effect of monopile-induced turbulence on local suspended sediment pattern around UK wind farms". In: (2018). URL: www.hull.ac.uk/iecs.

[48] Peter G Verity et al. *Grazing of phytoplankton by microzooplankton in the Barents Sea during early summer*. Tech. rep. 2002. URL: www.elsevier.com/locate/jmarsys.

[49] H K Versteeg and W Malalasekera. *An Introduction to Computational Fluid Dynamics Second Edition*. Tech. rep. 2007. URL: www.pearsoned.co.uk/versteeg.

[50] Paul Webb. *Introduction to Oceanography*. Tech. rep. 2023. URL: http://rwu.pressbooks.pub/webboceanography.

[51] *wetten.nl - Regeling - Kavelbesluit IV windenergiegebied Borssele - BWBR0037800*. URL: https://wetten.overheid.nl/BWBR0037800/2016-09-03.

[52] Windeurope. *Offshore Wind in Europe*. Tech. rep. 2020.

[53] Heng Xiao and Paola Cinnella. “Quantification of model uncertainty in RANS simulations: A review”. In: *Progress in Aerospace Sciences* 108 (2019), pp. 1–31. ISSN: 0376-0421. DOI: https://doi.org/10.1016/j.paerosci.2018.10.001. URL: https://www.sciencedirect.com/science/article/pii/S0376042118300952.

[54] Hongzhou Xu, Jing Lin, and Dongxiao Wang. “Numerical study on salinity stratification in the Pamlico River Estuary”. In: *Estuarine, Coastal and Shelf Science* 80.1 (Oct. 2008), pp. 74–84. ISSN: 02727714. DOI: 10.1016/j.ecss.2008.07.014.

[55] Yanyan Zhai and Erik Damgaard Christensen. “NUMERICAL INVESTIGATION OF FLOW IN POROUS MEDIA AROUND A MONO-PILE UNDER STEADY CURRENT”. In: *Proceedings of the International Conference on Offshore Mechanics and Arctic Engineering - OMAE*. Vol. 5-A. American Society of Mechanical Engineers (ASME), 2022. ISBN: 9780791885895. DOI: 10.1115/OMAE2022-79002.

[56] Jisheng Zhang et al. *Nested numerical simulation of muti-scale hydrodynamics 2 around monopile foundation of offshore wind farm at Weihai*. Tech. rep. 2023. URL: https://ssrn.com/abstract=4495247.